Journal of Proteomics 310 (2025) 105318

Contents lists available at ScienceDirect

Journal of Proteomics

journal homepage: www.elsevier.com/locate/jprot

# Tandem mass tag-based proteomic analysis of granulosa and theca interna cells of the porcine ovarian follicle following *in vitro* treatment with vitamin $D_3$ and insulin alone or in combination

Kinga Kamińska [a,b], Bianka Świderska [c], Agata Malinowska [c], Małgorzata Grzesiak [a,*]

[a] Department of Endocrinology, Institute of Zoology and Biomedical Research, Faculty of Biology, Jagiellonian University, Gronostajowa 9, 30-387 Krakow, Poland
[b] Doctoral School of Exact and Natural Sciences, Jagiellonian University, Krakow, Poland
[c] Mass Spectrometry Laboratory, Institute of Biochemistry and Biophysics, Polish Academy of Sciences, Pawinskiego 5a, 02-106 Warsaw, Poland

ARTICLE INFO

*Keywords:*
Vitamin $D_3$
Insulin
Granulosa cells
Theca interna cells
Liquid chromatography with tandem mass spectrometry
Cyclin dependent kinase 1
Scavenger receptor class B member 1

ABSTRACT

This study was performed to investigate the proteomic basis underlying the interaction between vitamin $D_3$ (VD) and insulin (I) within ovarian follicle using the pig as a model. Porcine antral follicles were incubated *in vitro* for 12 h with VD alone and I alone or in combination (VD + I) or with no treatment as the control (C). In total, 7690 and 7467 proteins were identified in the granulosa and theca interna compartments, respectively. Comparative proteomic analysis revealed 97 differentially abundant proteins (DAPs) within the granulosa layer and 11 DAPs within the theca interna layer. In the granulosa compartment, VD affected proteome leading to the promotion of cell proliferation, whereas I influenced mainly proteins related to cellular adhesion. The VD + I treatment induced granulosa cell proliferation probably *via* the DAPs involved in DNA synthesis and the cell cycle regulation. In the theca interna layer, VD alone or in co-treatment with I affected DAPs associated with cholesterol transport and lipid and steroid metabolic processes that was further confirmed by diminished lipid droplet accumulation.

*Significance:* The application of quantitative proteomics demonstrated for the first time the complexity of VD and I interactions in porcine ovarian follicle, providing a framework for understanding the molecular mechanisms underlying their cross-talk. Although identified DAPs were related to crucial ovarian processes, including the granulosa cell proliferation and cholesterol transport in the theca interna layer, novel molecular pathways underlying these processes have been proposed. The identified unique proteins may serve as indicators of VD and I interactions in both follicle layers, and could be useful biomarkers of ovarian pathologies characterized by impaired VD and I levels, such as polycystic ovary syndrome.

## 1. Introduction

The mammalian ovary performs two predominant functions: producing female germ cells and synthesizing steroid hormones required for successful reproduction [1]. The functional unit of the ovary is the ovarian follicle, which is composed of the oocyte surrounded by companion somatic cells such as granulosa cells and theca cells [2]. As the follicle grows, the granulosa cells extensively proliferate, forming an avascular layer that ensures an optimal intrafollicular milieu for oocyte maturation [1]. The theca cells create a vascularized layer adjacent to the basal lamina outside the granulosa cells, and this layer is differentiated into inner (theca interna) and outer (theca externa) compartments. These compartments provide androgens for estradiol production in the granulosa cells and structural support to the follicle, respectively [3]. Although the regulation of follicle development and function by pituitary gonadotropins and intraovarian molecules has been well established [4], there are still emerging factors that govern ovarian physiology and pathology and thereby influence female fertility.

*Abbreviations:* APOE, Apolipoprotein E; DAPs, Differentially Abundant Proteins; F11R, Transmembrane Junctional Adhesion Molecule 1; FC, Fold Change; FDR, False Discovery Rate; GO, Gene Ontology; I, Insulin; KEGG, Kyoto Encyclopedia of Genes and Genomes; KIF20A, Family Member 20A; LC-MS/MS, Liquid Chromatography with Tandem Mass Spectrometry; PCOS, Polycystic Ovary Syndrome; SCARB1, Scavenger Receptor Class B Member 1; STRING, Search Tool for the Retrieval of Interacting Genes/Proteins; TJP2, Cytoplasmic Scaffolding Tight Junction Protein 2; TMT, Tandem Mass Tag; VD, Vitamin $D_3$ ($1\alpha,25(OH)_2D_3$).

* Corresponding author at: Department of Endocrinology, Institute of Zoology and Biomedical Research, Jagiellonian University, Krakow, Poland.
*E-mail address:* m.e.grzesiak@uj.edu.pl (M. Grzesiak).

https://doi.org/10.1016/j.jprot.2024.105318
Received 19 June 2024; Received in revised form 8 September 2024; Accepted 11 September 2024
Available online 14 September 2024

Among multiple regulators of ovarian function in humans and animals, a growing body of research is highlighting the vital role of vitamin $D_3$ (VD) [5–7]. The ovary is an extrarenal site for the synthesis and metabolism of active VD ($1\alpha,25(OH)_2D_3$) *via* the expression of related enzymes such as CYP27B1 and CYP24A1 [8,9]. VD exerts its biological effects on ovarian cells by activating its receptors, namely nuclear VDR and membranous PDIA3, which are commonly expressed in granulosa and theca cells [6,9]. Investigations into the impact of VD on ovarian physiology have demonstrated its influence on folliculogenesis and steroidogenesis. To date, studies have shown that VD regulates preantral and antral follicle development *in vitro* in primates [10], induces the proliferation of caprine granulosa cells [11,12], and is associated with the maintenance of ovarian reserve in women [13]. Furthermore, VD directly regulates the expression and activity of steroidogenic enzymes and consequently steroid production in the ovaries of humans [14], pigs [9], and goats [11]. Given the importance of VD in ovarian processes, the emerging global deficiency and insufficiency of VD has the potential to attenuate female reproduction and contribute to reproductive disorders such as polycystic ovary syndrome (PCOS) [15,16].

PCOS is a common endocrinopathy that affects reproductive-age women and is characterized by at least two of the following hallmarks: clinical and/or biochemical hyperandrogenism, ovulatory dysfunction, and cystic ovarian morphology [17]. In addition to hormonal and reproductive disturbances leading to infertility, PCOS is often accompanied by metabolic abnormalities, especially insulin (I) resistance and hyperinsulinemia [18]. The ovary is a non-classical I target tissue [19], exhibiting a reduced I response in women with PCOS [20]. Although the beneficial effect of VD on the plasma I concentration and I sensitivity of classical tissues (*i.e.* liver, skeletal muscle and adipose tissue) has been demonstrated in PCOS [21], knowledge regarding the interaction between VD and I interaction at the ovary level remains incomplete.

Therefore, the objective of this study was to identify the proteomic background of VD and I interactions within the ovarian follicle, using the pig as a model and employing tandem mass tag (TMT)-labelled liquid chromatography-tandem mass spectrometry (LC-MS/MS). We hypothesized that the global proteome of porcine ovarian follicles exposed to VD and I, alone or in combination (VD + I), would differ from that of the control group. To verify this hypothesis, we examined the effect of VD, I and VD + I on the proteomic profile of the granulosa and theca interna layers of incubated *in vitro* porcine ovarian follicles for the first time. Such a holistic approach provides a unique opportunity to extend insight into the cross-talk between VD and insulin in the ovarian follicle, and it may indicate a new direction for future functional studies.

Notably, the pig is relevant as a model organism for biomedical research because of its human-like size, anatomy, and physiology, making it a promising alternative to rodents [22]. Furthermore, the availability of advanced omics tools justifies the increasing number of studies aimed at creating transcriptome/proteome catalogs for different porcine tissues, improving the usefulness of the pig model [23].

## 2. Materials and methods

### 2.1. Reagents

Phosphate-buffered saline (PBS) (cat. no. 14040–117), Pierce BCA Protein Assay Kit (cat. no. 23225), Pierce Quantitative Colorimetric Peptide Assay (cat. no. 23275), TMTpro 16-plex Label Reagent Set (cat. no. A44521) and Cy3-conjugated secondary anti-rabbit antibody (cat. no. A10520) were purchased from Thermo Fisher Scientific (Waltham, MA, USA). Medium M199 (cat. no. M4530), antibiotic–antimycotic solution (AAS 100×) (cat. no. A5955), deoxyribonuclease I from bovine pancreas (cat. no. D5025), fetal bovine serum (FBS) (heat-inactivated; cat. no. F9665), calcitriol ($1\alpha,25(OH)_2D_3$; cat. no. PHR1237), insulin (cat. no. I5523), and protease inhibitor cocktail (cat. no. P8849) were obtained from Sigma-Aldrich (St. Louis, MO, USA). Laemmli sample buffer (cat. no. 1610737) and Clarity Western ECL Substrate (cat. no. 170–5060) were purchased from Bio-Rad Laboratories (Hercules, CA, USA). β-Mercaptoethanol (cat. no. MER002) was purchased from Bioshop (Burlington, ON, Canada). Trypsin (cat. no. V5111) and CellTiter 96 AQueous One Solution Cell Proliferation Assay (cat. no. G358A) were purchased from Promega (Madison, WI, USA) and propidium iodide/RNase staining buffer (cat. no. 550825) was purchased from BD Biosciences (Franklin Lakes, NJ, USA). Vivacon 30 kDa molecular weight cut-off filter (cat. no. VN01H22) was obtained from Sartorius Stedim (Goettingen, Germany). Oasis HLB 1 cc Vac Cartridge, 30 mg Sorbent per Cartridge, 30 μm (cat. no. WAT094225) and XBridge Peptide BEH C18 column (cat. no. 186003581) were purchased from Waters (Milford, MA, USA). Analytical column (cat. no. EV1106) and Evotips C18 trap columns (cat. no. EV2003) were obtained from Evosep Biosystems (Odense, Denmark). VECTASHIELD Vibrance™ Antifade Mounting Medium with DAPI (cat. no. H-1800) was obtained from Vector Laboratories Inc. (Burlingame, CA, USA).

### 2.2. Materials

This study was conducted on porcine tissues obtained *post mortem* at a local abattoir. The use of animals complied with the Act of January 15, 2015 (Journal of Laws Dz. U. 2015 no. item 266) on the Protection of Animals Used for Scientific or Education Purposes, as well as Directive 2010/63/EU of the European Parliament and the Council of September 22, 2010 on the protection of animals used for scientific purposes.

Porcine ovaries were collected from healthy, sexually mature crossbred (Large White × Polish Landrace) gilts of similar age (6–8 months), weight (120–130 kg), and genetic background at a local slaughterhouse under veterinarian control. Within a few minutes after slaughter, the ovaries were removed, placed in cold PBS (pH 7.4) with AAS, and transported on ice to the laboratory within approximately 1 h. Healthy, medium-sized antral follicles (3.0–6.9 mm in diameter) were isolated from ovaries in the follicular phase of the estrous cycle. The stage of the estrous cycle was confirmed by ovarian morphology and corpus luteum quality [24,25].

### 2.3. In vitro culture and sample collection of ovarian follicles

An *in vitro* culture of porcine ovarian follicles was carried out as we previously described [25]. Briefly, whole ovarian follicles were individually placed in a Falcon Organ Culture Dish with a triangular stainless steel grid (Supplementary Fig. 1). First, the follicles were incubated in M199 medium supplemented with 1 % (*v*/v) FBS and AAS for 3 h (preincubation). Next, the culture medium was replaced with fresh M199 medium containing 0.1 % (v/v) FBS and AAS. The culture was then conducted for 12 h with medium alone as the control (C) or with the addition of VD ($1\alpha,25(OH)_2D_3$) (100 ng/mL) [9,26], I (10 ng/mL) [27], or the combination of VD and I (VD + I). All cultures were maintained at 37 °C in a humidified atmosphere of 5 % $CO_2$/95 % $O_2$. The experiment was repeated four time independently. In each replicate, six follicles from different animals per group were used.

After incubation, the granulosa and theca interna layers were mechanically separated. The ovarian follicles were transferred to a Petri dish with PBS and thoroughly rinsed. Each follicle was cut, and its wall was rinsed a few times with PBS to wash out the granulosa cells; this was followed by scrubbing with round-tripped ophthalmologic tweezers. Next, the remaining theca interna and externa layers were transferred to fresh PBS, and the theca interna was manually separated under a dissecting microscope using ophthalmologic tweezers [28]. The granulosa and theca interna cells obtained from six follicles were pooled into one sample ($n$ = 4 per group), centrifuged (1500 ×$g$ for 10 min at room temperature), snap-frozen and stored at −80 °C until total protein extraction. The purity of the granulosa and theca interna samples were confirmed by Western blot analysis of their marker proteins, namely cytochrome P450 aromatase (CYP19A1) and cytochrome P450 17α-

hydroxylase/c17,20-lyase (CYP17A1), respectively (Supplementary Fig. 3).

### 2.4. Protein extraction

The granulosa and theca interna samples were used for total protein extraction in lysis buffer (8 M urea, 2 % CHAPS, 30 mM TRIS-HCl; pH 8.0) with protease inhibitor cocktail. The samples were then homogenized on ice and sonicated. The lysates were centrifuged (12,000 ×*g* for 20 min at 4 °C), and the supernatants were collected for measurement of the protein concentration using Pierce BCA Protein Assay Kit with bovine serum albumin (BSA) as the standard according to the manufacturer's instructions.

### 2.5. Protein digestion

Each granulosa and theca interna sample containing 200 μg of protein was diluted to 120 μL with lysis buffer. Cysteine bridges were reduced by incubation with 10 mM Tris(2-carboxyethyl)phosphine (TCEP) for 1 h at 37 °C. The proteins were transferred onto a Vivacon 30 kDa molecular weight cut-off filter and digested according to the filter-aided sample preparation protocol with minor modifications [29]. The samples were spun at 14,500 ×*g* for 30 min and washed with 100 μL of 8 M urea solution in 200 mM triethylammonium bicarbonate buffer (TEAB) (pH 8.5) followed by cysteine blocking by a 15-min incubation with 20 mM *S*-methylmethanethiosulfonate (MMTS) at room temperature. The proteins were washed three times with 8 M urea solution and three times with 200 mM TEAB. After each addition, the samples were centrifuged until the cut-off filter was dry. Digestion was carried out overnight using trypsin in a 1:50 enzyme:protein ratio at 37 °C in 200 mM TEAB. Peptides were eluted from spin filters by two washes with 200 mM TEAB and one wash with 500 mM NaCl solution. The peptides were dried and resuspended in 100 μL of 200 mM TEAB buffer. Peptide concentrations were determined using the Pierce Quantitative Colorimetric Peptide Assay. In total, 70 μg of each peptide sample was labelled with TMTpro 16-plex tags in 20 μL acetonitrile (ACN) for 1 h on vortex. The reaction was quenched by the addition of 8 μL of 5 % (*w/v*) hydroxylamine. The labelling efficiency for each TMTpro set was checked using an Evosep One/Exploris 480 system with the method parameters described below. The samples were then combined, vacuum-dried and desalted using four 30 mg Oasis HLB columns for each sample set. Cartridges were activated with 1 mL of methanol and washed with 1 mL of MS-grade water. The samples were loaded and rinsed with 1 mL of 0.1 % (*v*/v) formic acid (FA) and 3 % (v/v) ACN. Peptides were eluted from the columns with 400 μL of 0.1 % (v/v) FA and 90 % (v/v) ACN. Aliquots were dried and resuspended in 500 μL of 3 % ACN in 10 mM ammonium hydroxide.

### 2.6. Reversed-phase peptide fractionation at high pH for LC-MS/MS

Labelled peptides were fractionated using high-pH reverse-phase chromatography on an XBridge Peptide BEH C18 column (4.6 × 250 mm, 130 Å, 5 μm) as previously described with some alterations to adjust the gradient for TMTpro tags [30]. Separation was performed at a flow rate 0.8 mL/min for 27 min on a Waters Acquity UPLC H-class system. The mobile phases consisted of water (A), ACN (B), and 100 mM ammonium hydroxide solution (C). The percentage of phase C was kept constant at 10 % through the entire gradient. Fractions were collected every 1 min starting from third minute of the run. The following gradient was applied: 3 % to 5 % solvent B for 0.5 min, 5 % to 22 % for 10.5 min, 22 % to 28 % for 7 min, 28 % to 50 % for 2.5 min, 50 % to 90 % for 0.5 min, 2.5-min isocratic hold at 90 %, 90 % to 5 % for 0.5 min, 5 % to 3 % for another 0.5 min, and the final column equilibration at 3 % phase B for 2.5 min. The peptide elution profile was monitored at 214 nm by an ultraviolet detector. Twenty five fractions from each TMTpro set were collected in deep-well 96-well plate, dried in SpeedVac, and reconstituted in 100 μL of 0.1 % (*v*/v) FA prior to LC-MS/MS analysis.

### 2.7. LC-MS/MS analysis

Peptide fractions were analyzed using an LC-MS/MS system composed of Evosep One (Evosep Biosystems) coupled to an Orbitrap Exploris 480 mass spectrometer (Thermo Fisher Scientific) *via* a Flex ion source (Thermo Fisher Scientific). Samples were loaded onto disposable Evotips C18 trap columns according to the manufacturer's protocol with minor modifications as described previously [31]. Briefly, Evotips were activated with 25 μL of Evosep solvent B (0.1 % (*v*/v) FA in ACN) by 1 min of centrifugation at 600 ×*g* followed by a 2-min incubation in 2-propanol. After equilibration with 25 μL of solvent A (0.1 % (v/v) FA in water), 10 μL of each sample solution was loaded onto the solid phase. Bound peptides were washed with 50 μL and covered with 300 μL of solvent A. Chromatography was carried out at a flow rate of 500 mL/min using a 44-min gradient (30 samples per day) on an analytical column (Dr Maisch C18 AQ, 1.9-μm beads, 150-μm inner diameter, 15-cm long). Data were acquired in positive mode using a data-dependent method with the following parameters. The MS1 resolution was set at 60,000 with a normalized automatic gain control target of 300 %, auto maximum inject time, and a scan range of 300 to 1550 *m/z*. For MS2, the resolution was set at 30,000 with a standard normalized automatic gain control target, auto maximum inject time, and the top 25 precursors within an isolation window of 1.2 m/z considered for MS/MS analysis. The TurboTMT resolution mode was set to "TMTpro Reagents". Dynamic exclusion was set at 20 s with an allowed mass tolerance of ±10 ppm, precursor intensity threshold of 5e3, and precursor fit threshold of 70 %. Precursors were fragmented in higher-energy collisional dissociation mode with a normalized collision energy of 30 %. The spray voltage was set to 2.1 kV, funnel radiofrequency level to 40, and heated capillary temperature to 275 °C.

### 2.8. Bioinformatic data analysis

Offline recalibration and peptide and protein identification were performed in the MaxQuant/Andromeda software suite (version 2.0.1.0) [32] using the *Sus scrofa* full UniProt database (version 2021_04, https://www.uniprot.org/). The search parameters included trypsin digestion with a maximum of two missed cleavages, methylthio (C) set as a fixed modification and oxidation (M) set as a variable modification. The mass tolerance for precursor ions was set as 20 ppm in the first search and 4.5 ppm in the main search respectively, and the fragment ion mass tolerance was defined as 0.2 Da. Reporter MS2 quantification was specified to obtain values for quantitative analysis. TMTpro 16plex correction factors were applied according to the manufacturer's datasheets. The reverse database was used for target/decoy statistical results validation, and the peptide and protein false discovery rate (FDR) was set to 0.01. The MS data are available in ProteomeXchange Consortium *via* the PRIDE partner repository with the dataset identifier PXD050533 and https://doi.org/10.6019/PXD050533.

Protein groups and quantitative data were further analyzed in R studio (version 4.2.2) using the Bioconductor "DEP" package (version 1.23.0) as extensively described at https://bioconductor.org/packages/devel/bioc/vignettes/DEP/inst/doc/DEP.html. Proteins identified only by site, repeated and duplicated proteins, and contaminants were removed from the dataset. Proteins with minimum number of two identified peptides per protein were used for the final analysis of differentially abundant proteins (DAPs). The data were normalized by Variance Stabilizing Normalization. Differential analysis was performed using protein-wise linear models combined with empirical Bayes moderated *t*-tests by the Bioconductor "limma" package. Multiple testing was corrected using the Benjamini-Hochberg FDR estimated by the R package "fdrtool". DAPs were identified based on a *p*-value adjusted (q-value) of < 0.05 and arbitrary fold change (FC) cut-off of ±1.5 [33,34]. The R package "ggplot2" and GraphPad Prism Software

version 8.0 (La Jolla, CA, USA) were used for data visualization. Following principal component analysis results, one outlier sample was removed from each examined group of granulosa and theca interna samples. Therefore, three replicates were used for further functional analyses of DAPs in both granulosa and theca interna samples (Supplementary Fig. 3). A Venn diagram was constructed at https://bioinformatics.psb.ugent.be/webtools/Venn/.

### 2.9. Functional analysis of DAPs

Gene Ontology (GO) analyses, including molecular function (MF), biological process (BP), and cellular component (CC), as well as Kyoto Encyclopedia of Genes and Genomes (KEGG) pathway enrichment analyses, were performed using the web server g:Profiler (version e109_eg56_p17_1d3191d, https://biit.cs.ut.ee/gprofiler/page/docs) to identify functional and pathway enrichment of DAPs [35]. g:Profiler was run by the *Sus scrofa* database, and enrichment analysis was carried out using g:GOSt with Benjamini-Hochberg FDR correction (q-value $<0.05$). Associations between DAPs were also identified using the Search Tool for the Retrieval of Interacting Genes database (STRING, version 12.0, https://string-db.org/) to better understand the functions of DAPs [36]. Protein-protein interactions (PPIs) were determined using a minimum required interaction score of 0.4. Because of the low number of DAPs identified in the theca interna layer, the STRING analysis was conducted only for DAPs in the granulosa layer.

### 2.10. Western blot analysis

To validate the proteomic results, the abundances of selected up- and down-regulated DAPs were validated using Western blot. The samples were denatured at 99.9 °C for 5 min in Laemmli sample buffer with β-mercaptoethanol, and an equal amount of protein (20 μg) from each sample was loaded onto the gel. Proteins were separated by 12 % (*w/v*) sodium dodecyl sulfate-polyacrylamide gel and transferred to polyvinylidene fluoride membranes using a semi-dry Trans-Blot Turbo Transfer System (Bio-Rad Laboratories). The membranes were washed and blocked in 5 % (w/v) non-fat dry milk containing 1 % (w/v) BSA and 0.1 % (*v*/v) Tween20. The membranes were then incubated overnight at 4 °C with monoclonal (for CDK1, CYP19A1, BCAT2 and SCARB1) or polyclonal (for AKR1C1, CYP11A1, CYP17A1, TPX2, RPL4 and RPL6) primary antibodies and with respective secondary horseradish peroxidase-conjugated antibodies for 1.5 h at room temperature (Table 1). Bands were detected by chemiluminescence using Western blotting Luminol Reagent and visualized using the ChemiDoc™ XRS+ System (Bio-Rad Laboratories). All membranes were stripped and re-probed with monoclonal anti-β-actin antibody followed by respective secondary antibody (Table 1). The relative intensities of protein bands were densitometrically quantified and normalized to their corresponding β-actin bands using the ImageJ software version 1.54d (National Institutes of Health, Bethesda, MD, USA). One–way ANOVA followed by Tukey's *post hoc* test was used to reveal differences between control and treated groups.

### 2.11. Isolation and culture of porcine granulosa cells

To analyze cell proliferation and cell cycle progression, granulosa cells were isolated from porcine medium antral follicles as described above in the section "*In vitro* culture and sample collection of ovarian follicles". The granulosa cells were exposed to deoxyribonuclease I (150 U for 1 min), washed in M199 medium, and then collected and resuspended in M199 medium supplemented with 10 % (*v*/v) FBS. The viability of the cells was determined using the trypan blue exclusion test and found to be >90 %. To measure cell proliferation, granulosa cells were inoculated at concentration of $5 \times 10^4$ cells/well in 96-well culture plates. To analyze the cell cycle, granulosa cells were seeded at concentration of $1 \times 10^6$ cells/well in six-well culture plates in M199 with 10 % (v/v) FBS. After 48 h of incubation, the medium was replaced by fresh medium containing 1 % (v/v) FBS and the following tested compounds: VD (100 ng/mL), I (10 ng/mL), or the two in combination (VD + I). The culture was then conducted in a humidified atmosphere at 37 °C with 5 % $CO_2$/95 % $O_2$ until further analyses. For each analysis, granulosa cells were collected from 8 to 12 follicles per biological repetition isolated from ovaries harvested from different animals.

**Table 1**
Primary and secondary antibodies used for Western blot.

| Antibody | Host species | Vendor | Catalog no. | RRID | Dilution |
|---|---|---|---|---|---|
| CYP19A1 | Mouse | Bio-Rad Laboratories, Berkeley, CA, USA | MCA2077S | AB_566942 | 1:500 |
| CYP17A1 | Rabbit | Gift from Professor Dale B. Hales, Southern Illinois University, Carbondale, USA | – | – | 1:1000 |
| CYP11A1 | Rabbit | Proteintech Group, Chicago, IL, USA | 13,363–1-AP | AB_2088552 | 1:1000 |
| AKR1C1 | Rabbit | ABclonal, Woburn, MA, USA | A13004 | AB_2759852 | 1:1000 |
| CDK1 | Rabbit | ABclonal, Woburn, MA, USA | A22347 | – | 1:1000 |
| RPL6 | Rabbit | Thermo Fisher Scientific, Waltham, MA, USA | PA5–30217 | AB_2547691 | 1:1000 |
| RPL4 | Rabbit | ABclonal, Woburn, MA, USA | A5886 | AB_2766634 | 1:1000 |
| SCARB1 | Rabbit | ABclonal, Woburn, MA, USA | A0827 | AB_2861480 | 1:1000 |
| TPX2 | Rabbit | Thermo Fisher Scientific, Waltham, MA, USA | PA3–16832 | AB_2208894 | 1:1000 |
| BCAT2 | Rabbit | ABclonal, Woburn, MA, USA | A23793 | – | 1:1000 |
| β-actin | Mouse | Sigma-Aldrich, St. Louis, MO, USA | A2228 | AB_476697 | 1:4000 |
| Secondary anti-rabbit IgG | Goat | Thermo Fisher Scientific, Waltham, MA, USA | 31,460 | AB_228341 | 1:3000 |
| Secondary anti-mouse IgG | Goat | Bio-Rad Laboratories, Berkeley, CA, USA | 170–6516 | AB_11125547 | 1:3000 |

Abbreviations: CYP19A1, cytochrome P450 aromatase; CYP17A1, cytochrome P450 17α-hydroxylase/17,20-lyase; CYP11A1, cholesterol side-chain cleavage enzyme; AKR1C1, aldo-keto reductase family 1 member C1; CDK1, cyclin dependent kinase 1; RPL6, 60S ribosomal protein L6; RPL4, 60S ribosomal protein L4; SCARB1, scavenger receptor class B member 1; TPX2, TPX2 microtubule nucleation factor; BCAT2, branched-chain-amino-acid aminotransferase, mitochondrial; RRID, Research Resource Identifiers.

### 2.12. Proliferation assay

A granulosa cell proliferation assay was performed after 12 h of incubation ($n = 6$) with VD and I alone or in combination (VD + I) using a CellTiter 96 AQueous One Solution Cell Proliferation Assay kit according to the manufacturer's protocol. CellTiter reagent (20 μL) was added to each well, and the plates were incubated in darkness in a humidified 5 % $CO_2$/95 % $O_2$ atmosphere at 37 °C for 3 h. Wells containing culture medium without cells and tested compounds incubated at the same conditions as samples were used as a blank. Reduction of the MTS tetrazolium compound to formazan was detected by colour development and measured at 490 nm using a spectrophotometer (Labtech LT-4500; Labtech, Heathfield, East Sussex, UK). One–way ANOVA followed by Tukey's *post hoc* test was used to find differences between the control and treated groups. The proliferation assay was performed six times independently.

### 2.13. Flow cytometry

Cell cycle analysis was performed after the granulosa cells had been incubated for 12 h ($n = 4$) with VD and I alone or in combination (VD + I). Before analysis, the medium and any floating, detached cells were removed prior to trypsinization (0.25 % (*v*/v) trypsin in PBS for 3 min at 37 °C). Next, the granulosa cells were washed twice in PBS, centrifuged (1500 ×*g* for 10 min at room temperature), fixed with cold methanol for 10 min and washed again in PBS. The pellet was resuspended in 400 μL of propidium iodide (PI)/RNase staining buffer and incubated for further 30 min at room temperature. Finally, the cell cycle was examined using a CytoFLEX flow cytometer with a blue laser (488 nm), detection filters 610/20 nm bandpass, and flow rate set to "medium" (Beckman Coulter, Brea, CA, USA). At least 10,000 cells were analyzed per sample. A negative control was set up with PBS alone (without PI). Kaluza 2.1.1 software (Beckman Coulter) was utilized to calculate the G0/G1, S and G2/M cell cycle phase distribution. Cell doublets were gated out on a PI peak *vs* PI width dotplot. One–way ANOVA followed by Tukey's *post hoc* test was used to identify differences between the control and treated groups. The analysis was repeated four times independently.

### 2.14. Immunofluorescence

Immunofluorescence labeling was performed to detect the SCARB1 protein in the theca interna layer of ovarian follicles after incubation with the tested compounds ($n = 3$). Briefly, formalin-fixed, paraffin-embedded, 5 μm thick porcine antral follicle sections were deparaffinized and rehydrated. The tissue sections were then subjected to microwave heating in 0.01 M citric buffer (pH 6.0) for epitope retrieval, then incubated with 5 % normal goat serum to block non-specific binding sites. Next, the sections were incubated overnight at 4 °C with primary anti-SCARB1 antibody (dilution 1:100) (see Table 1). Cy3-conjugated secondary anti-rabbit antibody (dilution 1:100) was then applied for 1.5 h in the dark at room temperature. Finally, the sections were coverslipped with VECTASHIELD Vibrance™ Antifade Mounting Medium with DAPI and visualized using an epifluorescence microscope (Nikon Eclipse Ni-U; Nikon, Tokyo, Japan) equipped with appropriate filters. No background fluorescence was observed in the negative control, where the primary antibody had been replaced by non-immune rabbit IgG.

Immunofluorescence images were quantified by determining the mean fluorescence intensity using ImageJ software version 1.54d [37]. Only the red channel was used to measure the fluorescence intensity of a region of interest corresponding to fluorescent labeling. Background subtraction was performed by measuring the fluorescence intensity of a non-fluorescent area. At least three randomly chosen sections from different follicles per each group were analyzed. One–way ANOVA followed by Tukey's *post hoc* test was used to find differences between the control and treated groups.

### 2.15. Transmission electron microscopy

Transmission electron microscopy was used to visualize and quantify lipid droplets (LDs) in the theca interna cells of the porcine ovarian follicles after *in vitro* incubation with the tested compounds. Whole ovarian follicles ($n = 4$) were cut into fragments and then fixed with 2.5 % (*v*/v) glutaraldehyde in 0.1 M cacodylic buffer (pH 7.4) with 3 mM $CaCl_2$ for 18 h at 4 °C. The samples were then post-fixed in a mixture of 1 % (*w*/*v*) osmium tetroxide and 3 % (w/v) potassium ferricyanide in 0.1 M cacodylic buffer at 4 °C for 1 h. After contrasting in 1 % uranyl acetate (v/v), the samples were dehydrated by passage through a graded ethanol series and propylene oxide. The dehydrated tissues were embedded in a PolyBed 812 Embedding Kit (Polysciences Inc., Warrington, PA, USA) at 60 °C. The tissue fragments were then cut into ultrathin sections using a Leica EM UC7 microtome, collected on copper grids, and contrasted using uranyl acetate and lead citrate. Within the obtained sections, theca interna cells were examined and photographed under electron microscope (JEM-2100HT; JEOL Ltd., Tokyo, Japan) operating at 80 kV and equipped with a 4 k × 4 k camera (T-VIPS, Oslo, Norway). Twenty randomly selected images (magnification 400×) of the theca interna layer per group were examined for LDs quantification using ImageJ software version 1.54d. The results are presented as the average number of LDs per cell. The nonparametric Kruskal-Wallis test was utilized, and the differences between groups were determined by Dunn's *post hoc* multiple comparison test.

### 2.16. Statistical analysis

Unless stated otherwise, statistical analysis was performed using GraphPad Prism Software version 8.0. To verify the distribution of data, the Shapiro–Wilk test was applied. In case of normal distribution of data, the parametric on-way ANOVA followed by Tukey's *post hoc* test was used, while due to the lack of normality, the nonparametric Kruskal-Wallis test followed by Dunn's *post hoc* multiple comparison test was utilized as stated above. Data are presented as the overall mean ± standard deviation, and differences were considered statistically significant at the 95 % confidence level ($p < 0.05$).

## 3. Results

### 3.1. Identification of DAPs in granulosa and theca interna layers

To analyze changes in the proteomic profile and identify DAPs (FC cutoff of 1.5 and a q-value of <0.05) within the granulosa and theca interna layers following VD, I, and VD + I treatment, a quantitative proteomic analysis was conducted using the TMT labeling LC-MS/MS technique. Quantitative analysis completed by MaxQuant software identified 7690 and 7467 proteins in the granulosa and theca interna layers, respectively. Next, 5894 and 5758 proteins, respectively from the granulosa and theca interna compartments, respectively, were further analyzed after the application of appropriate filters (proteins identified only by site, repeated and duplicated proteins, and contaminants were removed).

In the granulosa layer, 97 DAPs were identified between the examined groups (Table 2, Fig. 1A). The highest number of DAPs was observed in the comparisons VD *vs* VD + I and VD + I *vs* C (57 and 44 DAPs, respectively). In the VD *vs* VD + I group, 34 DAPs were up-regulated and 23 DAPs were down-regulated. In the VD + I *vs* C group, 24 DAPs were down-regulated and 20 DAPs were up-regulated. Only 14, 5, and 5 proteins were differentiated in the comparisons VD *vs* C (13 up-regulated and 1 down-regulated), I *vs* C (4 up-regulated and 1 down-regulated), and I *vs* VD + I (2 up-regulated and 3 down-regulated), respectively. The distribution of all DAPs was visualized in the volcano plots (Fig. 1B-F), and the normalized FC levels of these proteins were shown in a heatmap, which demonstrated hierarchical clustering between the experimental groups (Fig. 1H). In the VD *vs* VD +

**Table 2**
List of differentially abundant proteins (DAPs) identified in both the granulosa and theca interna layers of porcine ovarian follicles cultured *in vitro* from control (C), vitamin $D_3$ (VD), insulin (I), and both vitamin $D_3$ and insulin (VD + I) treated groups.

| | Gene name | Protein name | Changes | q-value | Fold change |
|---|---|---|---|---|---|
| GRANULOSA LAYER | | | | | |
| VD *vs* C | | | | | |
| 1. | NPR3 | Atrial natriuretic peptide receptor 3 isoform 1 | Down | 0.003 | −1.71 |
| 2. | AGXT2 | Alanine–glyoxylate aminotransferase 2 | Up | 0.0046 | 2.33 |
| 3. | CHI3L1 | Chitinase-3-like protein 1 | Up | 0.0123 | 1.86 |
| 4. | CA1 | Carbonic anhydrase | Up | 0.0005 | 1.83 |
| 5. | S100A6 | Protein S100-A6 | Up | 0.0363 | 1.76 |
| 6. | CLDN11 | Claudin 11 | Up | 0.0464 | 1.68 |
| 7. | COL12A1 | Collagen type XII alpha 1 chain | Up | 0.0471 | 1.66 |
| 8. | MYH11 | Myosin-11 | Up | 0.0003 | 1.64 |
| 9. | RGS3 | RGS domain-containing protein | Up | 0.0003 | 1.57 |
| 10. | CEMIP | Hyaluronoglucosaminidase | Up | 0.0009 | 1.54 |
| 11. | DIAPH3 | Diaphanous related formin 3 | Up | 0.0193 | 1.52 |
| 12. | ZEB1 | Zinc finger *E*-box binding homeobox 1 | Up | 0.0003 | 1.52 |
| 13. | MARCKSL1 | Myristoylated alanine rich protein kinase C substrate like 1 | Up | 0.0406 | 1.51 |
| 14. | S100A13 | Protein S100-A13 | Up | 0.0023 | 1.50 |
| I *vs* C | | | | | |
| 1. | F11R | Junctional adhesion molecule 1 | Down | 0.0476 | −1.56 |
| 2. | UNC93B1 | Unc-93 homolog B1, TLR signaling regulator | Up | 0.0029 | 2.36 |
| 3. | TJP2 | Tight junction protein 2 | Up | $1.41 \times 10^{-9}$ | 1.64 |
| 4. | CAV1 | Caveolin-1 | Up | 0.0232 | 1.60 |
| 5. | CELSR2 | Cadherin EGF LAG seven-pass G-type receptor 2 | Up | 0.0033 | 1.58 |
| VD + I *vs* C | | | | | |
| 1. | ORM1 | Alpha-1-acid glycoprotein | Down | 0.0002 | −2.55 |
| 2. | ATP1B1 | Sodium/potassium-transporting ATPase subunit beta-1 | Down | 0.0111 | −2.25 |
| 3. | A1BG | Alpha-1B-glycoprotein | Down | 0.0015 | −2.06 |
| 4. | F11R | Junctional adhesion molecule 1 | Down | $2.53 \times 10^{-6}$ | −1.99 |
| 5. | APOR | Apolipoprotein R | Down | 0.0332 | −1.93 |
| 6. | DPP4 | Dipeptidyl peptidase 4 | Down | 0.0306 | −1.92 |
| 7. | HRG | Histidine rich glycoprotein | Down | 0.0077 | −1.91 |
| 8. | CYP11A1 | Cholesterol side-chain cleavage enzyme. Mitochondrial | Down | 0.0004 | −1.91 |
| 9. | AKR1C1 | Aldo-keto reductase family 1 member C1 | Down | 0.0318 | −1.90 |
| 10. | MAP2 | Microtubule-associated protein | Down | 0.0391 | −1.89 |
| 11. | GABARAPL1 | GABA type A receptor associated protein like 1 | Down | 0.0005 | −1.73 |
| 12. | NPR3 | Atrial natriuretic peptide receptor 3 isoform 1 | Down | 0.0286 | −1.66 |
| 13. | PAM | Peptidyl-glycine alpha-amidating monooxygenase isoform X1 | Down | 0.0415 | −1.65 |
| 14. | CTSC | Cathepsin C | Down | 0.0207 | −1.64 |
| 15. | TNFAIP8L3 | TNF alpha induced protein 8 like 3 | Down | 0.0013 | −1.63 |
| 16. | SNAP23 | Synaptosomal-associated protein | Down | 0.0146 | −1.61 |
| 17. | CREG1 | Cellular repressor of E1A stimulated genes 1 | Down | 0.0385 | −1.59 |
| 18. | RAB27B | Small monomeric GTPase | Down | 0.0397 | −1.59 |
| 19. | SLC2A3 | Solute carrier family 2, facilitated glucose transporter member 3 | Down | 0.0417 | −1.58 |
| 20. | FAM102B | Family with sequence similarity 102 member B | Down | 0.0387 | −1.57 |
| 21. | AHSG | Alpha-2-HS-glycoprotein | Down | 0.0229 | −1.57 |
| 22. | BASP1 | Brain acid soluble protein 1 | Down | 0.0374 | −1.56 |
| 23. | JUNB | Transcription factor jun-B | Down | 0.0490 | −1.54 |
| 24. | PSAP | Prosaposin | Down | 0.0084 | −1.53 |
| 25. | NES | Nestin | Up | 0.0238 | 2.07 |
| 26. | ANLN | Anillin actin binding protein | Up | 0.0002 | 2.06 |
| 27. | FANCD2 | FA complementation group D2 | Up | 0.0178 | 1.99 |
| 28. | CA1 | Carbonic anhydrase | Up | 0.0125 | 1.89 |
| 29. | DUT | Deoxyuridine 5-triphosphate nucleotidohydrolase | Up | 0.0067 | 1.79 |
| 30. | ZNF185 | Zinc finger protein 185 with LIM domain | Up | 0.0104 | 1.79 |
| 31. | STRA6 | Receptor for retinol uptake STRA6 | Up | 0.0342 | 1.73 |
| 32. | WDHD1 | WD repeat and HMG-box DNA binding protein 1 | Up | 0.0197 | 1.72 |
| 33. | KIF11 | Kinesin family member 11 | Up | 0.0377 | 1.71 |
| 34. | CHAF1A | Chromatin assembly factor 1 subunit A | Up | 0.0008 | 1.70 |
| 35. | TPX2 | TPX2 microtubule nucleation factor | Up | 0.0001 | 1.70 |
| 36. | NUSAP1 | Nucleolar and spindle associated protein 1 | Up | $2.16 \times 10^{-5}$ | 1.69 |
| 37. | ERCC6L | DNA excision repair protein ERCC-6-like isoform a | Up | 0.0014 | 1.64 |
| 38. | POLA1 | DNA polymerase alpha catalytic subunit | Up | 0.0008 | 1.63 |
| 39. | CKAP2 | Cytoskeleton associated protein 2 | Up | 0.0321 | 1.58 |
| 40. | TJP2 | Tight junction protein 2 | Up | $4.92 \times 10^{-8}$ | 1.57 |
| 41. | HELB | DNA helicase B | Up | 0.0291 | 1.55 |
| 42. | SPC24 | Kinetochore protein Spc24 | Up | 0.0076 | 1.54 |
| 43. | TACC3 | Transforming acidic coiled-coil containing protein 3 | Up | 0.0218 | 1.53 |
| 44. | IQGAP3 | IQ motif containing GTPase activating protein 3 | Up | 0.0002 | 1.51 |
| VD *vs* VD + I | | | | | |
| 1. | FANCD2 | FA complementation group D2 | Down | 0.0024 | −2.60 |
| 2. | ANLN | Anillin actin binding protein | Down | $2.59 \times 10^{-5}$ | −2.53 |
| 3. | SHCBP1 | SHC binding and spindle associated 1 | Down | 0.0112 | −2.22 |
| 4. | KIF11 | Kinesin family member 11 | Down | 0.0070 | −2.13 |
| 5. | CHAF1A | Chromatin assembly factor 1 subunit A | Down | $5.46 \times 10^{-5}$ | −2.04 |

(*continued on next page*)

**Table 2** (*continued*)

| | Gene name | Protein name | Changes | q-value | Fold change |
|---|---|---|---|---|---|
| 6. | PRC1 | Protein regulator of cytokinesis 1 | Down | 0.0004 | −2.01 |
| 7. | CKAP2 | Cytoskeleton associated protein 2 | Down | 0.0034 | −1.94 |
| 8. | ERCC6L | DNA excision repair protein ERCC-6-like isoform a | Down | 0.0001 | −1.93 |
| 9. | TPX2 | TPX2 microtubule nucleation factor | Down | $7.08 \times 10^{-5}$ | −1.88 |
| 10. | CDK1 | Cyclin dependent kinase 1 | Down | 0.0337 | −1.86 |
| 11. | NUSAP1 | Nucleolar and spindle associated protein 1 | Down | $7.97 \times 10^{-5}$ | −1.79 |
| 12. | IQGAP3 | IQ motif containing GTPase activating protein 3 | Down | $7.70 \times 10^{-6}$ | −1.74 |
| 13. | TIMELESS | Protein timeless homolog | Down | $8.15 \times 10^{-7}$ | −1.74 |
| 14. | SPC24 | Kinetochore protein Spc24 | Down | 0.0017 | −1.74 |
| 15. | NUF2 | NUF2 component of NDC80 kinetochore complex | Down | 0.0286 | −1.70 |
| 16. | POLA1 | DNA polymerase | Down | 0.0043 | −1.67 |
| 17. | DLGAP5 | DLG associated protein 5 | Down | 0.0001 | −1.64 |
| 18. | CENPF | Centromere protein F | Down | 0.0173 | −1.63 |
| 19. | NOC4L | Nucleolar complex associated 4 homolog | Down | 0.0456 | −1.58 |
| 20. | KIF15 | Kinesin family member 15 | Down | $2.51 \times 10^{-5}$ | −1.58 |
| 21. | NCAPH | Condensin complex subunit 2 | Down | 0.0165 | −1.53 |
| 22. | ATAD2 | ATPase family AAA domain containing 2 | Down | 0.0288 | −1.51 |
| 23. | KIF20A | Kinesin family member 20 A | Down | 0.0292 | −1.50 |
| 24. | ORM1 | Alpha-1-acid glycoprotein | Up | $6.40 \times 10^{-7}$ | 4.03 |
| 25. | MSMB | Beta-microseminoprotein | Up | 0.0293 | 3.20 |
| 26. | LGALS3 | Galectin | Up | 0.0342 | 2.83 |
| 27. | A1BG | Alpha-1B-glycoprotein | Up | 0.0001 | 2.62 |
| 28. | F10 | Coagulation factor X | Up | 0.0129 | 2.39 |
| 29. | F2 | Prothrombin | Up | 0.0419 | 2.39 |
| 30. | S100A6 | Protein S100-A6 | Up | 0.0377 | 2.38 |
| 31. | CLDN11 | Claudin 11 | Up | 0.0263 | 2.36 |
| 32. | NPC2 | Epididymal secretory protein E1 | Up | 0.0386 | 2.33 |
| 33. | DPP4 | Dipeptidyl peptidase 4 | Up | 0.0158 | 2.31 |
| 34. | FILIP1L | Filamin A interacting protein 1 like | Up | 0.0123 | 2.31 |
| 35. | PLAUR | Urokinase plasminogen activator surface receptor | Up | 0.0039 | 2.27 |
| 36. | APOA1 | Apolipoprotein A-I | Up | 0.0285 | 1.97 |
| 37. | LAGE3 | L antigen family member 3 | Up | 0.0111 | 1.94 |
| 38. | HRG | Histidine rich glycoprotein | Up | 0.0293 | 1.94 |
| 39. | GABARAPL1 | GABA type A receptor associated protein like 1 | Up | 0.0004 | 1.90 |
| 40. | NAB2 | NGFI-A binding protein 2 | Up | 0.0213 | 1.87 |
| 41. | DKK3 | Dickkopf WNT signaling pathway inhibitor 3 | Up | 0.0041 | 1.86 |
| 42. | RAB27B | Small monomeric GTPase | Up | 0.0190 | 1.82 |
| 43. | F11R | Junctional adhesion molecule 1 | Up | 0.0020 | 1.81 |
| 44. | NDRG1 | N-myc downstream-regulated gene 1 protein | Up | 0.0231 | 1.78 |
| 45. | FHL1 | Four and a half LIM domains 1 | Up | 0.0006 | 1.69 |
| 46. | STOM | Stomatin | Up | 0.0011 | 1.69 |
| 47. | PSAP | Prosaposin | Up | 0.0053 | 1.68 |
| 48. | STX4 | Syntaxin 4 | Up | 0.0431 | 1.67 |
| 49. | VAT1 | Synaptic vesicle membrane protein VAT-1 homolog | Up | 0.0408 | 1.67 |
| 50. | PLIN2 | Perilipin-2 | Up | 0.0293 | 1.66 |
| 51. | PROS1 | Vitamin K-dependent protein S | Up | 0.0490 | 1.64 |
| 52. | SELENBP1 | Selenium binding protein 1 | Up | 0.0005 | 1.63 |
| 53. | FOLH1B | Folate hydrolase 1 | Up | $9.94 \times 10^{-5}$ | 1.62 |
| 54. | SLC44A2 | Choline transporter-like protein 2 | Up | 0.0246 | 1.61 |
| 55. | GSTP1 | GST class-pi | Up | 0.0159 | 1.61 |
| 56. | MICAL1 | F-actin monooxygenase | Up | 0.0249 | 1.58 |
| 57. | MFGE8 | Lactadherin | Up | 0.0454 | 1.51 |
| I *vs* VD + I | | | | | |
| 1. | RPL6 | 60S ribosomal protein L6 | Down | 0.0233 | −1.79 |
| 2. | RPL4 | 60S ribosomal protein L4 | Down | 0.0276 | −1.62 |
| 3. | NUSAP1 | Nucleolar and spindle associated protein 1 | Down | 0.0299 | −1.53 |
| 4. | APOR | Apolipoprotein R | Up | 0.0005 | 3.01 |
| 5. | APOA1 | Apolipoprotein A-I | Up | 0.0294 | 2.07 |
| TECA INTERNA LAYER | | | | | |
| VD *vs* C | | | | | |
| 1. | SCARB1 | Scavenger receptor class B member 1 | Down | 0.0031 | −1.55 |
| 2. | RPL6 | 60S ribosomal protein L6 | Down | 0.0313 | −1.50 |
| 3. | CA1 | Carbonic anhydrase | Up | $1.11 \times 10^{-6}$ | 2.00 |
| 4. | EXT2 | Exostosin glycosyltransferase 2 | Up | 0.0003 | 1.51 |
| VD + I *vs* C | | | | | |
| 1. | BCAT2 | Branched-chain-amino-acid aminotransferase, mitochondrial | Down | 0.0071 | −1.72 |
| 2. | CA1 | Carbonic anhydrase | Up | 0.0001 | 2.19 |
| 3. | APON | Ovarian and testicular apolipoprotein N | Up | 0.0217 | 1.83 |
| 4. | HBB | Hemoglobin subunit beta | Up | $3.07 \times 10^{-5}$ | 1.62 |
| 5. | LOC110259958 | GLOBIN domain-containing protein | Up | 0.0005 | 1.59 |
| 6. | CLU | Clusterin | Up | 0.0342 | 1.59 |
| 7. | EXT2 | Exostosin glycosyltransferase 2 | Up | 0.0080 | 1.58 |
| 8. | SLC4A1 | Anion exchange protein | Up | 0.0437 | 1.52 |
| I *vs* VD + I | | | | | |
| 1. | CA1 | Carbonic anhydrase | Down | 0.0201 | −2.10 |
| 2. | PLAT | Tissue-type plasminogen activator | Up | 0.0212 | 1.57 |

The list contains all DAPs identified in the granulosa layer of VD *vs* C, I *vs* C, VD + I *vs* C, VD *vs* VD + I, and I *vs* VD + I groups and in the theca interna layer of VD *vs* C, VD + I *vs* C, and I *vs* VD + I groups. The table includes the gene name, full protein name, fold change and q-value of each DAP. DAPs were identified by R analysis of the LC-MS/MS results using parameters such as q-values of $<0.05$ and fold changes of $\leq -1.5$ or $\geq 1.5$.

I, VD *vs* C, and I *vs* VD + I groups, the DAPs expression profiles were similar. The profiles in the I *vs* C and VD + I *vs* C groups exhibited the same trend. A Venn diagram was created to illustrate the overlapping DAPs between the examined groups, showing that 17 DAPs were differentially abundant in both the VD *vs* VD + I and VD + I *vs* C comparisons (Fig. 1G).

In the theca interna layer, 11 DAPs were identified between the examined groups (Table 2, Fig. 2A). The comparison between the VD + I and C groups revealed the highest number of DAPs, totaling 8. Among them, 7 DAPs were up-regulated and 1 DAP was down-regulated. Additionally, LC/MS-MS analysis showed 4 DAPs in the VD *vs* C group (2 up-regulated and 2 down-regulated) and 2 DAPs in the I *vs* VD + I group (1 up-regulated and 1 down-regulated). The distribution of all identified DAPs was visualized in volcano plots (Fig. 2B-D), and the normalized FC levels of these proteins were shown in a heatmap, which depicted hierarchical clustering between the analyzed groups (Fig. 2F). In the VD *vs* C, VD *vs* VD + I, and I *vs* VD + I groups, the DAP expression profiles were similar, and the profiles revealed the same trend in the VD + I *vs* C and I *vs* C groups. A Venn diagram illustrated that one of the identified DAPs was differentially abundant in all comparisons (VD *vs* C, VD + I *vs* C, and I *vs* VD + I) and that another DAP was differentially abundant in two comparisons (VD *vs* C and VD + I *vs* C) (Fig. 2E).

### 3.2. Functional enrichment of DAPs identified in granulosa and theca interna layers

To elucidate the possible functions of DAPs identified within the granulosa and theca interna layers following VD, I, and VD + I treatment, proteins were assigned to functional ontology annotations and classified into three main categories: biological process (BP), molecular function (MF) and cellular component (CC), according to the GO database and the KEGG enrichment pathway (Figs. 3A-E, 4A-C). The 10 crucial subcategories (q-value $<0.05$) assigned for each of three main GO and KEEG annotations are presented in tables (Figs. 3A'-E', 4A'-C').

In the granulosa layer, the DAPs identified in the comparison VD *vs* C assigned to the MF category were "calcium-dependent protein binding", "carbonate dehydratase activity", and "molecular function". Those assigned to the BP category were "cellular process", "biological process", "developmental process", and "cellular component organization". That assigned to the CC category was "perinuclear region of cytoplasm". According to the KEGG enrichment analysis, the identified DAPs also had a possible role in tight junction (TJ) formation and regulation of the actin cytoskeleton (Fig. 3A, A'). The comparison of the I *vs* C group showed that single DAPs were assigned to "transmembrane transporter binding" and "integrin binding" within the MF category; to "membrane raft organization", "negative regulation of molecular function", "cellular response to mechanical stimulus", "negative regulation of endothelial cell proliferation", and "cell adhesion" within the BP category; and to "tight junction" and "cell-cell junction" within the CC category. According to the KEGG database, the DAPs were enriched in "tight junction" (Fig. 3B, B'). In the comparison of VD + I *vs* C, the DAPs were ascribed mainly to "binding" and "molecular function" within the MF category; to "cell cycle", "cellular process", "response to stress", "metabolic process", and "selective autophagy" within the BP category; to "non-membrane-bounded organelle" and "cellular component" within the CC category; and to "ovarian steroidogenesis" according to the KEGG enrichment pathway (Fig. 3C, C'). The DAPs identified in the comparison between the VD and VD + I groups were assigned to "microtubule binding" and "protein binding" within the MF category; to "cell cycle", "microtubule cytoskeleton organization involved in mitosis", "organelle organization", "response to stress", "oocytes maturation", "reproductive process", and "antral ovarian follicle growth" within the BP category; and to "non-membrane-bounded organelle" within the CC category (Fig. 3D, D'). The comparison of the I *vs* VD + I group revealed single DAPs annotated to "high-density lipoprotein particle receptor binding" and "phosphatidylcholine-sterol O-acyltransferase activator activity" within the MF category; to "reverse cholesterol transport", "regulation of sterol transport", "positive regulation of small molecule metabolic process", "sterol biosynthetic process", and "mitotic cytokinesis" within the BP category; to "lipoprotein particle" and "mitotic spindle" within the CC category; and to "ribosome" according to the KEGG database (Fig. 3E, E').

In the theca interna layer, the DAPs identified in the comparison VD *vs* C were enriched mainly in "carbonate dehydratase activity", "scavenger receptor activity", and "carbon-oxygen lyase activity" within the MF category; in "cholesterol transport", "one-carbon metabolic process", "cell recognition", and "endocytosis" within the BP category; in "membrane raft" and "caveola" within the CC category; and in "ribosome" according to the KEGG database (Fig. 4A, A'). The DAPs identified in the comparison VD + I *vs* C were predominantly associated with steroidogenic processes through the annotation to "estradiol 17-beta-dehydrogenase [NAD(P)] activity", "steroid dehydrogenase activity, acting on the CH-OH group of donors, NAD or NADP as acceptor", "oxidoreductase activity", and "steroid dehydrogenase activity" within the MF category, as well as "steroid metabolic process", "lipid metabolic process", "sterol metabolic process" and "small molecule metabolic process" within the BP category and "basal part of cell" in the CC category. Based on the KEGG enrichment analysis, one DAP was annotated to "2-oxocarboxylic acid metabolism" (Fig. 4B, B'). In the I *vs* VD + I comparison, the DAPs were enriched in "carbonate dehydratase activity", "carbon-oxygen lyase activity", "hydro-lyase activity", and "endopeptidase activity" within the MF category and in "plasminogen activation", "one-carbon metabolic process", "protein processing", and "protein maturation" within the BP category. According to the KEGG enrichment analysis, the DAPs were also assigned to "nitrogen metabolism" and "apelin signaling pathway" (Fig. 4C, C').

### 3.3. STRING network analysis of DAPs identified in granulosa layer

The network of PPIs within the granulosa layer was established by submitting the identified DAPs to the STRING database. Functional networks were obtained for the comparisons I *vs* C, VD + I *vs* C, and VD *vs* VD + I. The remaining input proteins devoid of any interactions were excluded from the network (Fig. 5). The functional classification of DAPs in the comparison I *vs* C produced a PPI network with 5 nodes and 2 edges. Only the "cell-cell junction" (GO:0005911) category (2 DAPs; q-value = 0.0486) confirmed the data obtained by g:Profiler (Fig. 5A). In the comparison VD + I *vs* C, the functional classification of DAPs generated a PPI network with 43 nodes and 46 edges. "Cell cycle" (GO:0007049) was one of the most enriched GO terms, containing 14 DAPs (q-value = $2.72 \times 10^{-5}$) (Fig. 5B). In the VD *vs* VD + I comparison, the DAP network contained 57 nodes and 143 edges. Among them, 26 DAPs were categorized to the "protein binding" GO term (GO:0005515, q-value = 0.0013), in agreement with g:Profiler. In addition, "cell cycle" (GO:0007049, q-value = $2.54 \times 10^{-8}$) and "microtubule cytoskeleton organization involved in mitosis" (GO:1902850, q-value = 0.00078), also revealed by g:Profiler, were among the enriched GO terms, including 19 and 6 DAPs, respectively (Fig. 5C). Interestingly, 6 DAPs (DLGA5P, KIF11, NUF2, NUSAP1, PRC1, and TPX2) were shared between these 3 enriched GO terms and 8 DAPs (ANLN, CDK1, CENPF, CHAF1A, FANCD2, IQGAP3, KIF20A, and TIMELESS) were classified into "cell cycle" and "binding protein".

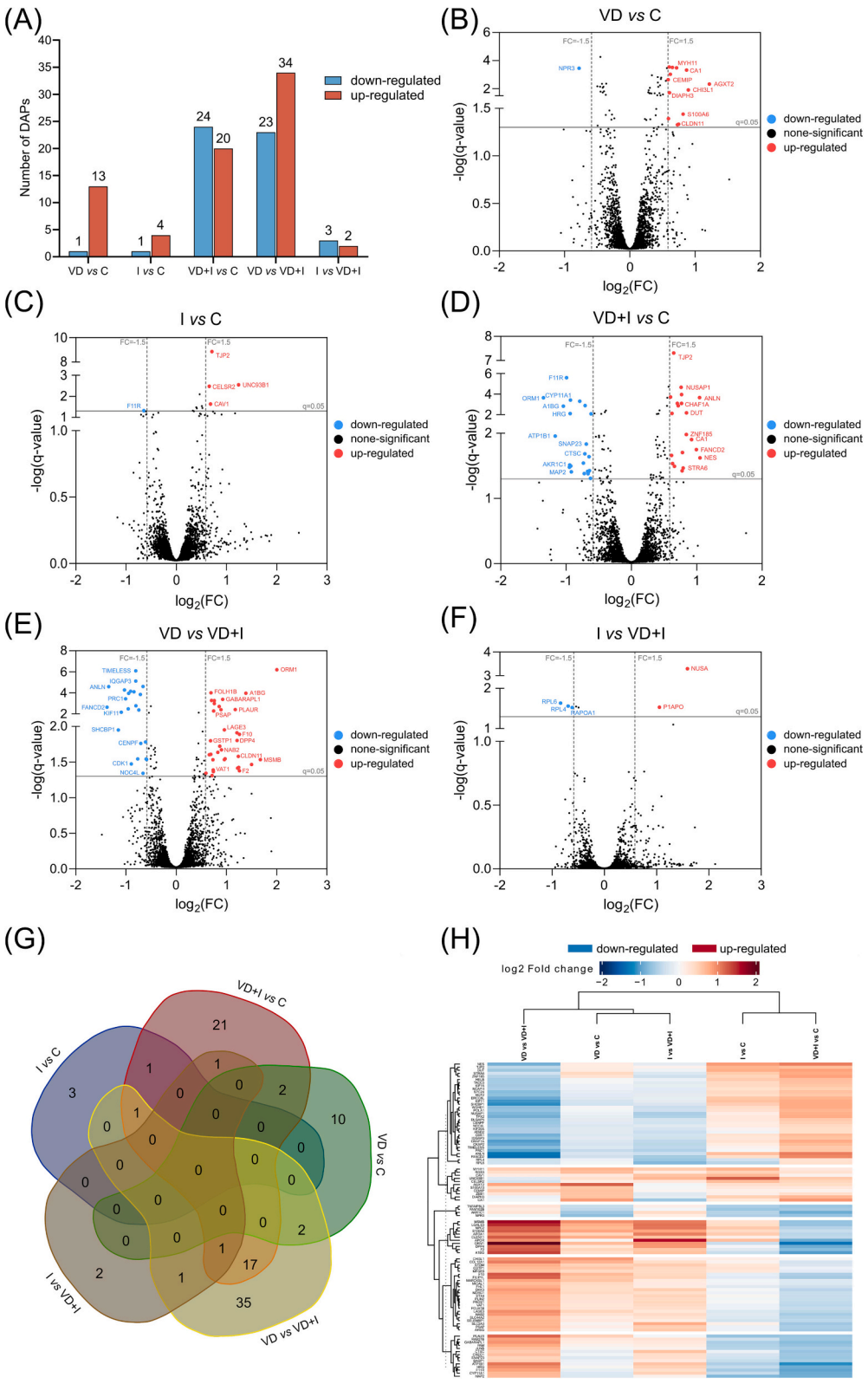


**Fig. 1.** Profile of differentially abundant proteins (DAPs) in the granulosa layer of porcine ovarian follicles cultured *in vitro* from control (C), vitamin $D_3$ (VD), insulin (I), and both vitamin $D_3$ and insulin (VD + I) treated groups. **(A)** Total numbers of up- and down-regulated DAPs identified in VD *vs* C, I *vs* C, VD + I *vs* C, VD *vs* VD + I and I *vs* VD + I groups. (B—F) Volcano plot representations of DAPs [fold change (FC) $\leq -1.5$ and $\geq 1.5$, q-value <0.05] showing the distribution of significance [−log(q-value)] *vs* FC [log2(FC)] for all identified proteins between the examined groups. Down-regulated DAPs are marked in blue, up-regulated DAPs are marked in red, and non-significant DAPs are marked in black. **(G)** Venn diagram depicting the overlap of DAPs in VD *vs* C, I *vs* C, VD + I *vs* C, VD *vs* VD + I and I *vs* VD + I groups. **(H)** Heatmap and hierarchical clustering analysis of DAPs in VD *vs* VD + I, VD *vs* C, I *vs* VD + I, I *vs* C, and VD + I *vs* C groups. Each row shows the relative expression presented as $\log_2$ fold change of protein and each column represents a group of comparisons, in which down-regulated proteins are marked in blue, and up-regulated proteins are marked in red. (For interpretation of the references to colour in this figure legend, the reader is referred to the web version of this article.)

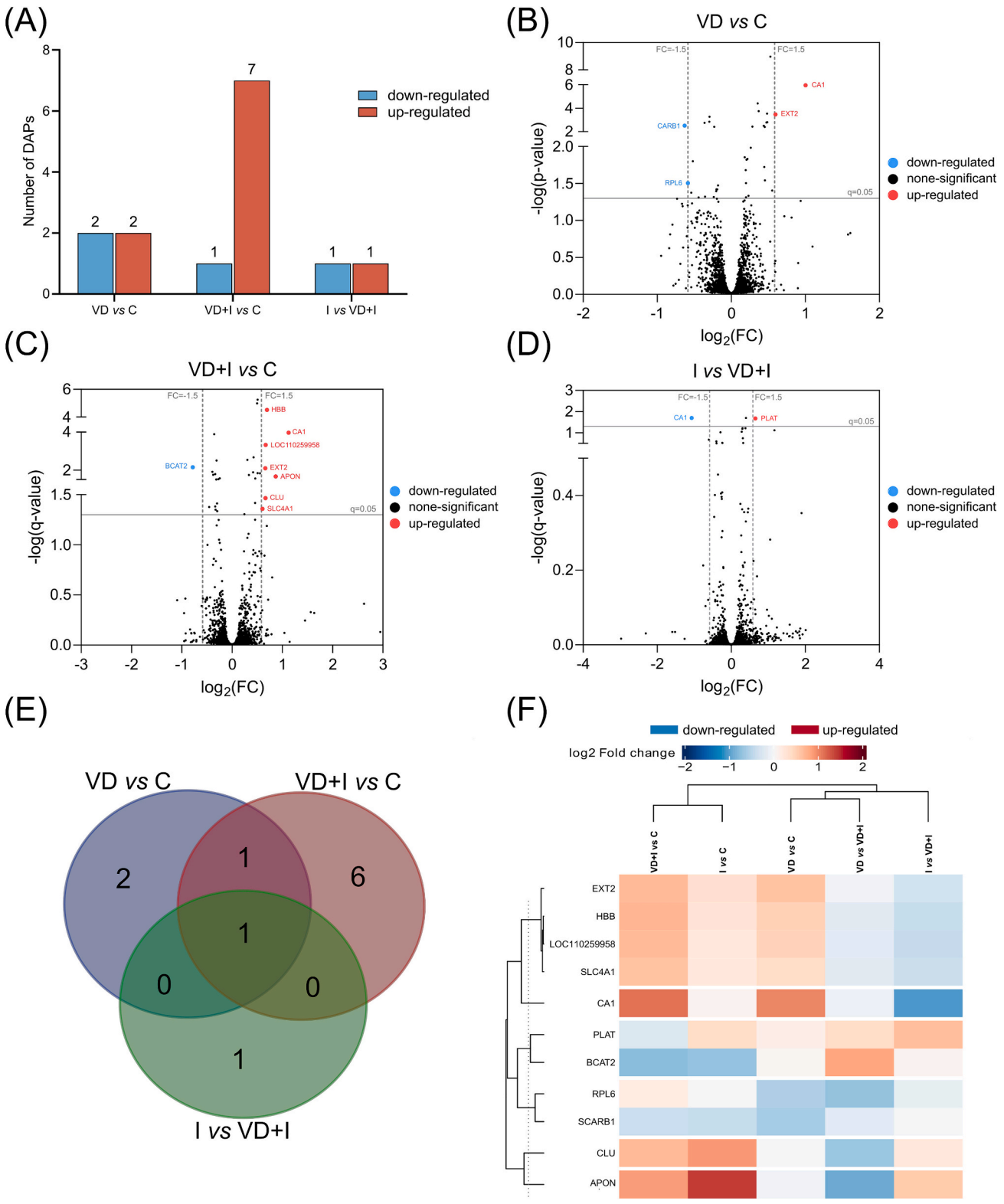


**Fig. 2.** Profiles of differentially abundant proteins (DAPs) in the theca interna layer of porcine ovarian follicles cultured *in vitro* from control (C), vitamin $D_3$ (VD), insulin (I), and both vitamin $D_3$ and insulin (VD + I) treated groups. **(A)** Total numbers of up- and down-regulated DAPs identified in VD *vs* C, VD + I *vs* C and I *vs* VD + I groups. **(B—D)** Volcano plot representations of DAPs [fold change (FC) $\leq -1.5$ and $\geq 1.5$, q-value $<0.05$] showing distribution of significance [−log(q-value)] *vs* FC [log2(FC)] for all identified proteins between the examined groups. Down-regulated DAPs are marked in blue, up-regulated DAPs are marked in red, and non-significant DAPs are marked in black. **(E)** Venn diagram depicting the overlap of DAPs in VD *vs* C, VD + I *vs* C and I *vs* VD + I groups. **(F)** Heatmap and hierarchical clustering analysis of DAPs in VD + I *vs* C, I *vs* C, VD *vs* C, VD *vs* VD + I, and I *vs* VD + I groups. Each row shows the relative expression presented as $\log_2$ fold change of protein and each column represents a group of comparisons, in which down-regulated proteins are marked in blue, and up-regulated proteins are marked in red. (For interpretation of the references to colour in this figure legend, the reader is referred to the web version of this article.)

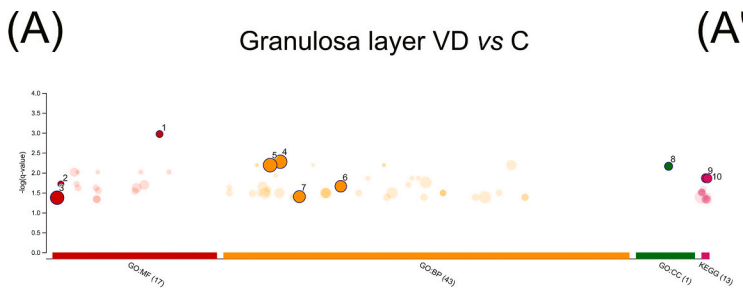


(A')

| ID | Source | Term ID | Term name | q-value | Protein size | Proteins |
|---|---|---|---|---|---|---|
| 1. | GO:MF | GO:0048306 | Calcium-dependent protein binding | 0.0011 | 2 | S100A6, S100A13 |
| 2. | GO:MF | GO:0004089 | Carbonate dehydratase activity | 0.0192 | 1 | CA1 |
| 3. | GO:MF | GO:0003674 | Molecular_function | 0.0423 | 8 | AGXT2, CA1, S100A6, MYH11, ZEB1, MARCKSL1, S100A13, NPR3 |
| 4. | GO:BP | GO:0009987 | Cellular process | 0.0053 | 11 | AGXT2, CA1, CLDN11, COL12A1, MYH11, RGS3, DIAPH3, ZEB1, MARCKSL1, S100A13, NPR3 |
| 5. | GO:BP | GO:0008150 | Biological_process | 0.0064 | 11 | AGXT2, CA1, CLDN11, COL12A1, MYH11, RGS3, DIAPH3, ZEB1, MARCKSL1, S100A13, NPR3 |
| 6. | GO:BP | GO:0032502 | Developmental process | 0.0218 | 4 | COL12A1, MYH11, ZEB1, MARCKSL1 |
| 7. | GO:BP | GO:0016043 | Cellular component organization | 0.0397 | 4 | CLDN11, MYH11, DIAPH3, MARCKSL1 |
| 8. | GO:CC | GO:0048471 | Perinuclear region of cytoplasm | 0.0069 | 2 | S100A6, S100A13 |
| 9. | KEGG | KEGG:04530 | Tight junction | 0.0137 | 2 | CLDN11, MYH11 |
| 10. | KEGG | KEGG:04810 | Regulation of actin cytoskeleton | 0.0137 | 2 | MYH11, DIAPH3 |

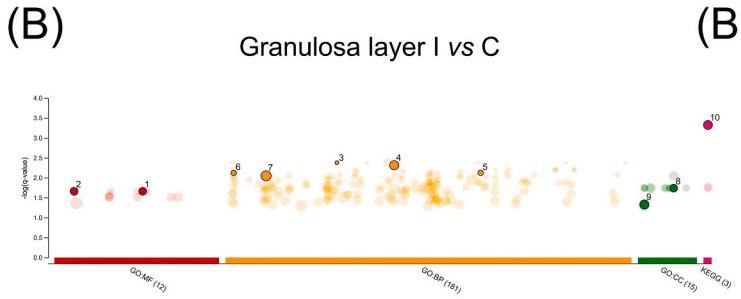


(B')

| ID | Source | Term ID | Term name | q-value | Protein size | Proteins |
|---|---|---|---|---|---|---|
| 1. | GO:MF | GO:0044325 | Transmembrane transporter binding | 0.0219 | 1 | CAV1 |
| 2. | GO:MF | GO:0005178 | Integrin binding | 0.0219 | 1 | F11R |
| 3. | GO:BP | GO:0031579 | Membrane raft organization | 0.0042 | 1 | CAV1 |
| 4. | GO:BP | GO:0044092 | Negative regulation of molecular function | 0.0049 | 2 | F11R, CAV1 |
| 5. | GO:BP | GO:0071260 | Cellular response to mechanical stimulus | 0.0075 | 1 | F11R |
| 6. | GO:BP | GO:0001937 | Negative regulation of endothelial cell proliferation | 0.0075 | 1 | CAV1 |
| 7. | GO:BP | GO:0007155 | Cell adhesion | 0.0090 | 2 | F11R, CELSR2 |
| 8. | GO:CC | GO:0070160 | Tight junction | 0.0183 | 1 | F11R |
| 9. | GO:CC | GO:0005911 | Cell-cell junction | 0.0470 | 1 | F11R |
| 10. | KEGG | KEGG:04530 | Tight junction | 0.0005 | 2 | F11R, TJP2 |

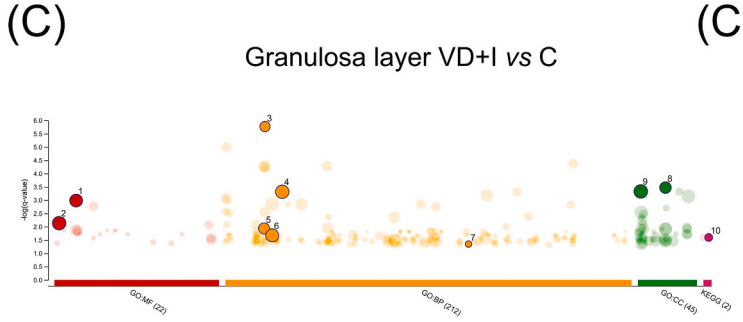


(C')

| ID | Source | Term ID | Term name | q-value | Protein size | Proteins |
|---|---|---|---|---|---|---|
| 1. | GO:MF | GO:0005488 | Binding | 0.0010 | 17 | NES, FANCD2, DUT, WDHD1, TPX2, NUSAP1, POLA1, HELB, SPC24, JUNB, BASP1, SNAP23, NPR3, GABARAPL1, MAP2, HRG, F11R |
| 2. | GO:MF | GO:0003674 | Molecular_function | 0.0073 | 22 | NES, FANCD2, CA1, DUT, WDHD1, KIF11, TPX2, NUSAP1, ERCC6L, POLA1, HELB, SPC24, PSAP, JUNB, BASP1, SNAP23, CTSC, NPR3, GABARAPL1, MAP2, HRG, F11R |
| 3. | GO:BP | GO:0007049 | Cell cycle | 1.70E-06 | 9 | ANLN, FANCD2, WDHD1, KIF11, TPX2, NUSAP1, POLA1, SPC24, JUNB |
| 4. | GO:BP | GO:0009987 | Cellular process | 0.0005 | 24 | NES, ANLN, FANCD2, CA1, DUT, STRA6, WDHD1, KIF11, TPX2, NUSAP1, POLA1, HELB, SPC24, TACC3, PSAP, JUNB, BASP1, SNAP23, NPR3, GABARAPL1, MAP2, AKR1C1, HRG, F11R |
| 5. | GO:BP | GO:0006950 | Response to stress | 0.0116 | 6 | FANCD2, WDHD1, HELB, GABARAPL1, HRG, F11R |
| 6. | GO:BP | GO:0008152 | Metabolic process | 0.0212 | 14 | FANCD2, CA1, DUT, WDHD1, POLA1, HELB, PSAP, JUNB, BASP1, CTSC, GABARAPL1, AKR1C1, HRG, F11R |
| 7. | GO:BP | GO:0061912 | Selective autophagy | 0.0449 | 1 | GABARAPL1 |
| 8. | GO:CC | GO:0043228 | Non-membrane-bounded organelle | 0.0003 | 10 | NES, ANLN, FANCD2, WDHD1, KIF11, TPX2, NUSAP1, POLA1, HELB, SPC24 |
| 9. | GO:CC | GO:0005575 | Cellular_component | 0.0005 | 25 | NES, ANLN, FANCD2, CA1, STRA6, WDHD1, KIF11, TPX2, NUSAP1, POLA1, HELB, SPC24, TACC3, PSAP, JUNB, BASP1, CREG1, SNAP23, TNFAIP8L3, CTSC, GABARAPL1, MAP2, HRG, F11R, ORM1 |
| 10. | KEGG | KEGG:04913 | Ovarian steroidogenesis | 0.0254 | 2 | AKR1C1, CYP11A1 |

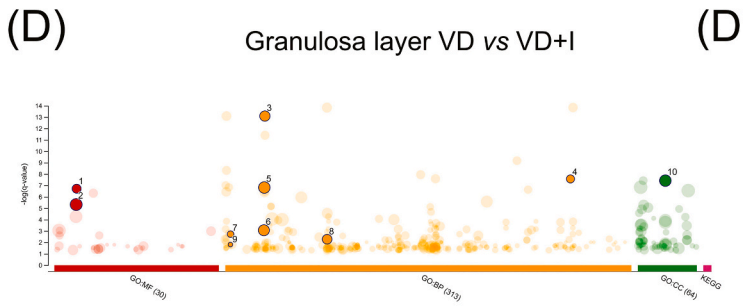


(D')

| ID | Source | Term ID | Term name | q-value | Protein size | Proteins |
|---|---|---|---|---|---|---|
| 1. | GO:MF | GO:0008017 | Microtubule binding | 1.94E-07 | 7 | KIF20A, KIF15, DLGAP5, SPC24, NUSAP1, TPX2, PRC1 |
| 2. | GO:MF | GO:0005515 | Protein binding | 4.76E-06 | 16 | S100A6, APOA1, GABARAPL1, DKK3, F11R, FHL1, MICAL1, KIF20A, ATAD2, KIF15, DLGAP5, SPC24, NUSAP1, TPX2, PRC1, FANCD2 |
| 3. | GO:BP | GO:0007049 | Cell cycle | 8.14E-14 | 15 | KIF20A, NCAPH, CENPF, DLGAP5, POLA1, NUF2, SPC24, TIMELESS, NUSAP1, CDK1, TPX2, PRC1, KIF11, ANLN, FANCD2 |
| 4. | GO:BP | GO:1902850 | Microtubule cytoskeleton organization involved in mitosis | 2.68E-08 | 6 | DLGAP5, NUF2, NUSAP1, TPX2, PRC1, KIF11 |
| 5. | GO:BP | GO:0006996 | Organelle organization | 1.53E-07 | 15 | GABARAPL1, F11R, VAT1, MICAL1, KIF20A, NCAPH, DLGAP5, NUF2, NUSAP1, CDK1, TPX2, PRC1, KIF11, ANLN, FANCD2 |
| 6. | GO:BP | GO:0006950 | Response to stress | 0.0009 | 8 | F10, F2, HRG, GABARAPL1, F11R, TIMELESS, CDK1, FANCD2 |
| 7. | GO:BP | GO:0001556 | Oocyte maturation | 0.0019 | 2 | KIF20A, CDK1 |
| 8. | GO:BP | GO:0022414 | Reproductive process | 0.0053 | 4 | KIF20A, NUF2, CDK1, FANCD2 |
| 9. | GO:BP | GO:0001547 | Antral ovarian follicle growth | 0.0155 | 1 | KIF20A |
| 10. | GO:CC | GO:0043228 | Non-membrane-bounded organelle | 3.80E-08 | 16 | PLIN2, MICAL1, KIF20A, KIF15, CENPF, DLGAP5, POLA1, NUF2, SPC24, TIMELESS, NUSAP1, TPX2, PRC1, KIF11, ANLN, FANCD2 |

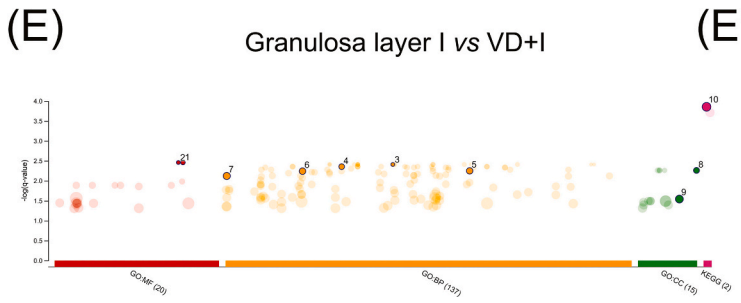


(E')

| ID | Source | Term ID | Term name | q-value | Protein size | Proteins |
|---|---|---|---|---|---|---|
| 1. | GO:MF | GO:0070653 | High-density lipoprotein particle receptor binding | 0.0035 | 1 | APOA1 |
| 2. | GO:MF | GO:0060228 | Phosphatidylcholine-sterol O-acyltransferase activator activity | 0.0035 | 1 | APOA1 |
| 3. | GO:BP | GO:0043691 | Reverse cholesterol transport | 0.0039 | 1 | APOA1 |
| 4. | GO:BP | GO:0032371 | Regulation of sterol transport | 0.0044 | 1 | APOA1 |
| 5. | GO:BP | GO:0062013 | Positive regulation of small molecule metabolic process | 0.0056 | 1 | APOA1 |
| 6. | GO:BP | GO:0016126 | Sterol biosynthetic process | 0.0057 | 1 | APOA1 |
| 7. | GO:BP | GO:0000281 | Mitotic cytokinesis | 0.0076 | 1 | NUSAP1 |
| 8. | GO:CC | GO:1990777 | Lipoprotein particle | 0.0055 | 1 | APOA1 |
| 9. | GO:CC | GO:0072686 | Mitotic spindle | 0.0287 | 1 | NUSAP1 |
| 10. | KEGG | KEGG:03010 | Ribosome | 0.0001 | 2 | RPL4, RPL6 |

**Fig. 3.** g:Profiler functional enrichment analysis of differentially abundant proteins (DAPs) in the granulosa layer of porcine ovarian follicles cultured *in vitro* from control (C), vitamin $D_3$ (VD), insulin (I), and both vitamin $D_3$ and insulin (VD + I) treated groups. Manhattan plots illustrate the results of Gene Ontology (GO) analysis of DAPs identified in **(A)** VD *vs* C, **(B)** I *vs* C, **(C)** VD + I *vs* C, **(D)** VD *vs* VD + I, and **(E)** I *vs* VD + I groups, where the X-axis shows the functional terms, and the Y-axis represents the −log(q-value). Functional terms are grouped and colour-coded based on their data sources as follows: molecular function (MF; in red), biological processes (BP; in orange), cellular components (CC; in green) and Kyoto Encyclopedia of Genes and Genomes (KEGG; in pink). The tables **(A'-E')** present the detailed results of 10 crucial enriched representative terms marked by a number in the respective Manhattan plot. Only terms with a Benjamini-Hochberg q-value of $<0.05$ are shown in the graphs. Detailed representation and annotation of all proteins submitted to the analysis can be found in Supplementary Table 5. (For interpretation of the references to colour in this figure legend, the reader is referred to the web version of this article.)

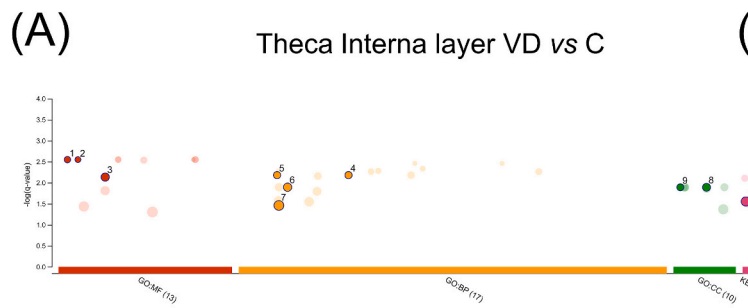


(A')

| ID | Source | Term ID | Term name | q-value | Protein size | Proteins |
|---|---|---|---|---|---|---|
| 1. | GO:MF | GO:0004089 | Carbonate dehydratase activity | 0.0028 | 1 | CA1 |
| 2. | GO:MF | GO:0005044 | Scavenger receptor activity | 0.0028 | 1 | SCARB1 |
| 3. | GO:MF | GO:0016835 | Carbon-oxygen lyase activity | 0.0073 | 1 | CA1 |
| 4. | GO:BP | GO:0030301 | Cholesterol transport | 0.0066 | 1 | SCARB1 |
| 5. | GO:BP | GO:0006730 | One-carbon metabolic process | 0.0066 | 1 | CA1 |
| 6. | GO:BP | GO:0008037 | Cell recognition | 0.0128 | 1 | SCARB1 |
| 7. | GO:BP | GO:0006897 | Endocytosis | 0.0347 | 1 | SCARB1 |
| 8. | GO:CC | GO:0045121 | Membrane raft | 0.0128 | 1 | SCARB1 |
| 9. | GO:CC | GO:0005901 | Caveola | 0.0128 | 1 | SCARB1 |
| 10. | KEGG | KEGG:03010 | Ribosome | 0.0279 | 1 | RPL6 |

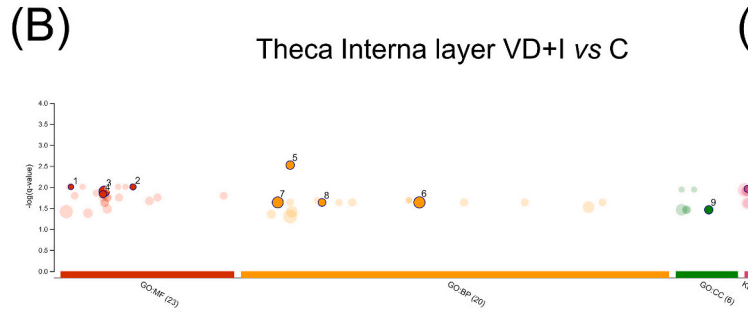


(B')

| ID | Source | Term ID | Term name | q-value | Protein size | Proteins |
|---|---|---|---|---|---|---|
| 1. | GO:MF | GO:0004303 | Estradiol 17-beta-dehydrogenase [NAD(P)] activity | 0.0099 | 1 | BCAT2 |
| 2. | GO:MF | GO:0033764 | Steroid dehydrogenase activity, acting on the CH-OH group of donors, NAD or NADP as acceptor | 0.0099 | 1 | BCAT2 |
| 3. | GO:MF | GO:0016491 | Oxidoreductase activity | 0.0127 | 2 | LOC110259958, BCAT2 |
| 4. | GO:MF | GO:0016229 | Steroid dehydrogenase activity | 0.0148 | 1 | BCAT2 |
| 5. | GO:BP | GO:0008202 | Steroid metabolic process | 0.0030 | 2 | APON, BCAT2 |
| 6. | GO:BP | GO:0044281 | Small molecule metabolic process | 0.0231 | 2 | CA1, APON |
| 7. | GO:BP | GO:0006629 | Lipid metabolic process | 0.0231 | 2 | APON, BCAT2 |
| 8. | GO:BP | GO:0016125 | Sterol metabolic process | 0.0231 | 1 | APON |
| 9. | GO:CC | GO:0045178 | Basal part of cell | 0.0346 | 1 | SLC4A1 |
| 10. | KEGG | KEGG:01210 | 2-Oxocarboxylic acid metabolism | 0.0110 | 1 | BCAT2 |

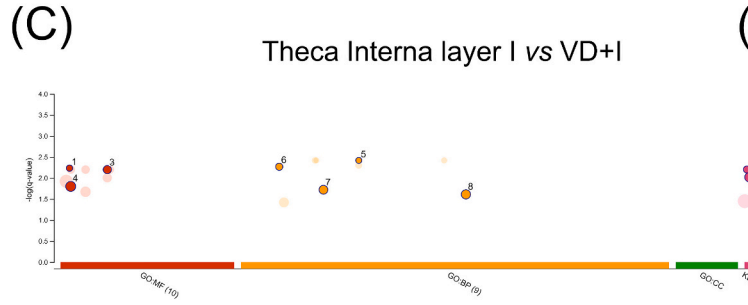


(C')

| ID | Source | Term ID | Term name | q-value | Protein size | Proteins |
|---|---|---|---|---|---|---|
| 1. | GO:MF | GO:0004089 | Carbonate dehydratase activity | 0.0058 | 1 | CA1 |
| 2. | GO:MF | GO:0016835 | Carbon-oxygen lyase activity | 0.0063 | 1 | CA1 |
| 3. | GO:MF | GO:0016836 | Hydro-lyase activity | 0.0063 | 1 | CA1 |
| 4. | GO:MF | GO:0004175 | Endopeptidase activity | 0.0158 | 1 | PLAT |
| 5. | GO:BP | GO:0031639 | Plasminogen activation | 0.0038 | 1 | PLAT |
| 6. | GO:BP | GO:0006730 | One-carbon metabolic process | 0.0054 | 1 | CA1 |
| 7. | GO:BP | GO:0016485 | Protein processing | 0.0190 | 1 | PLAT |
| 8. | GO:BP | GO:0051604 | Protein maturation | 0.0245 | 1 | PLAT |
| 9. | KEGG | KEGG:00910 | Nitrogen metabolism | 0.0063 | 1 | CA1 |
| 10. | KEGG | KEGG:04371 | Apelin signaling pathway | 0.0096 | 1 | PLAT |

**Fig. 4.** g:Profiler functional enrichment analysis of differentially abundant proteins (DAPs) in the theca interna layer of porcine ovarian follicles cultured *in vitro* from control (C), vitamin $D_3$ (VD), insulin (I), and both vitamin $D_3$ and insulin (VD + I) treated groups.
Manhattan plots illustrate the results of Gene Ontology (GO) analysis of DAPs identified in **(A)** VD *vs* C, **(B)** VD + I *vs* C, and **(C)** I *vs* VD + I groups, where the X-axis shows the functional terms, and the Y-axis represents the −log(q-value). Functional terms are grouped and colour-coded based on their data sources as follows: molecular function (MF; in red), biological processes (BP; in orange), cellular components (CC; in green) and Kyoto Encyclopedia of Genes and Genomes (KEGG; in pink). The tables **(A'-C')** present the detailed results of 10 crucial enriched representative terms marked by a number in the respective Manhattan plot. Only terms with a Benjamini-Hochberg q-value of <0.05 are shown in the graphs. Detailed representation and annotation of all proteins submitted to the analysis can be found in Supplementary Table 6. (For interpretation of the references to colour in this figure legend, the reader is referred to the web version of this article.)

### *3.4. Validation of LC-MS/MS data by Western blot*

To validate the data from the TMT-based LC-MS/MS analysis, the abundance of several candidate proteins (6 for the granulosa layer and 2 for the theca interna layer) were examined by Western blot, and the results were compared with the findings from the proteomic analysis (Fig. 6). Regarding DAPs identified in the granulosa layer, Western blot analysis revealed decreased abundance of AKR1C1 and CYP11A1 proteins ($p < 0.05$ and $p < 0.01$, respectively) in the VD + I group relative to the C group (Fig. 6A' and B′, respectively). The abundance of CDK1 protein was greater in the VD + I group than in the VD group ($p < 0.05$) (Fig. 6C'), whereas TPX2 protein was more abundant in the VD + I group than in the C and VD groups ($p < 0.05$) (Fig. 6D'). In addition, the abundance of RPL6 and RPL4 protein was increased in the VD + I group relative to the I group ($p < 0.05$) (Fig. 6E' and F′, respectively). Regarding DAPs identified in the theca interna layer, the abundance of SCARB1 protein was decreased in the VD group when relative to the C group ($p < 0.05$) (Fig. 6G'), while the abundance of BCAT2 protein was lower in the VD + I group than in the C group ($p < 0.05$) (Fig. 6H'). The abundances of all selected DAPs obtained by Western blot confirmed the LC-MS/MS results (Fig. 6A-H).

### *3.5. Validation of LC-MS/MS data by proliferation assay and cell cycle analysis of granulosa cells*

Considering the results of the functional analysis of DAPs identified in the granulosa layer, additional functional tests (proliferation assay and flow cytometry cell cycle analysis) were performed to validate the LC-MS/MS data (Fig. 7). Porcine granulosa cells were treated *in vitro* with VD, I, and VD + I for 12 h in both analyses.

Granulosa cell proliferation was expressed as a percentage relative to the control. The analysis showed a significant increase in the proliferation rate of granulosa cells in the VD and VD + I groups relative to the C group ($p < 0.05$ and $p < 0.01$, respectively) (Fig. 7A). Flow cytometry analysis revealed that the VD and VD + I groups had a significant increased percentage of granulosa cells in the S phase of the cell cycle relative to the C group ($p < 0.05$) (Fig. 7B, C). However, the population of granulosa cells in the G0/G1 and G2/M phases of the cell cycle did not show significant changes after *in vitro* incubation with the tested compounds.

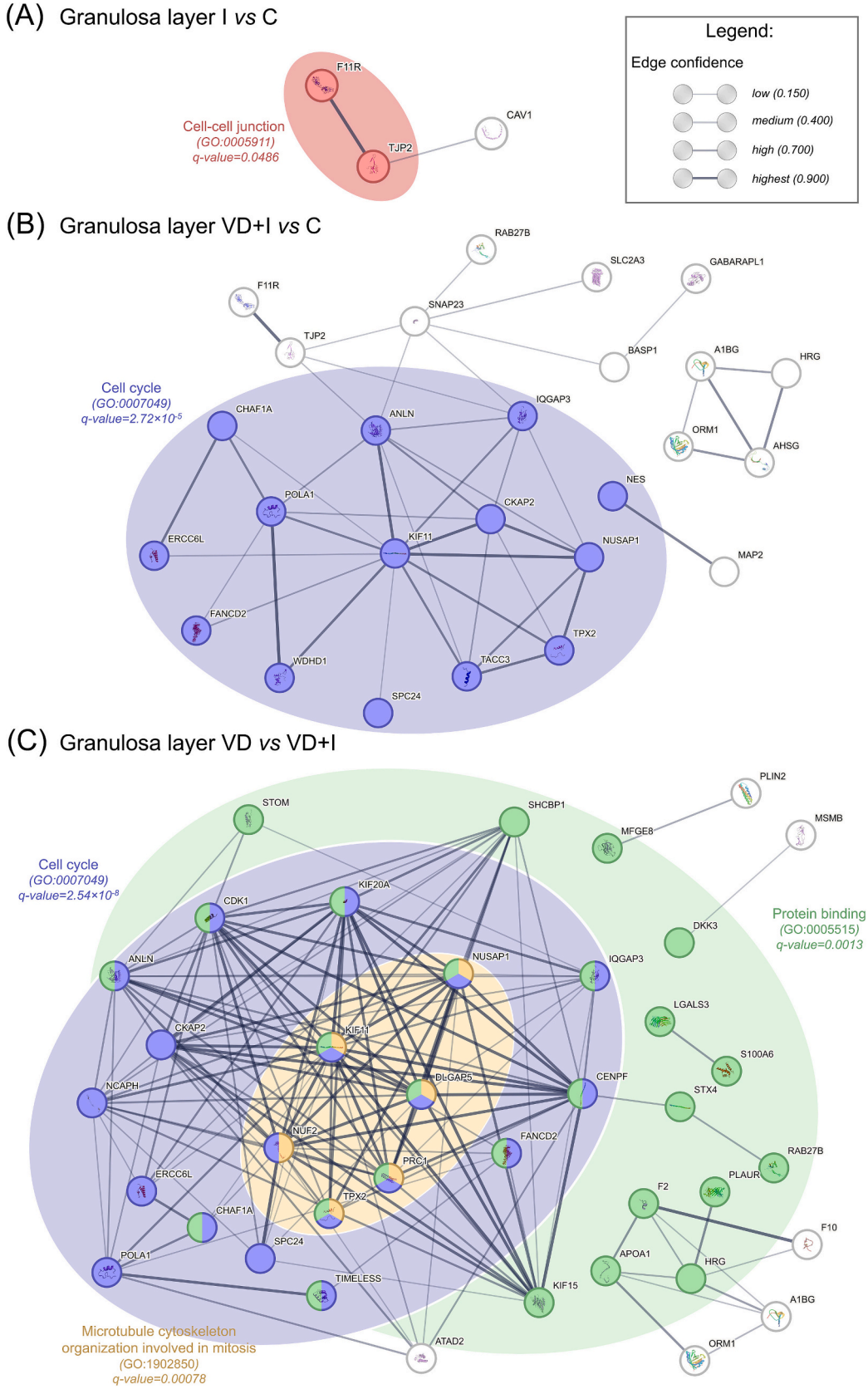


*(caption on next page)*

**Fig. 5.** Predicted protein-protein interaction networks of differentially abundant proteins (DAPs) identified in the granulosa layer of porcine ovarian follicles cultured *in vitro* from control (C), vitamin $D_3$ (VD), insulin (I), and both vitamin $D_3$ and insulin (VD + I) treated groups.
The analysis was performed according to the STRING database using a minimum required interaction score of 0.4 in the following groups: **(A)** I *vs* C, **(B)** VD + I *vs* C, and **(C)** VD *vs* VD + I with enrichment *p*-values of 0.00213, $1.0 \times 10^{-16}$, and $1.0 \times 10^{-16}$, respectively. The nodes in the graphs represent different proteins, and the interactions among them are indicated by edges. The thickness of the edges reflects the degree of confidence in the protein–protein interaction. Detected protein interactions in the clusters of interest are marked with different colors: cell-cell junction (GO:0005911) in red, cell cycle (GO:0007049) in blue, protein binding (GO:0005515) in green and microtubule cytoskeleton organization involved in mitosis (GO:1902850) in yellow. (For interpretation of the references to colour in this figure legend, the reader is referred to the web version of this article.)

### *3.6. Validation of LC-MS/MS data by SCARB1 immunofluorescence and LDs visualization in theca interna cells*

Additional validation was conducted based on the results obtained from the functional analysis of the identified DAPs within the theca interna layer. First, SCARB1 immunofluorescent localization in the theca interna layer was performed with quantitative analysis of fluorescence intensity (Fig. 8A, A'). Considering that SCARB1 is involved in the cholesterol uptake, we subsequently used transmission electron microscopy to visualize LDs in theca interna cells and determine their accumulation (Fig. 8B, B'). Throughout both analyses, whole porcine ovarian follicles were treated with VD, I, and combination of VD + I for 12 h, focusing solely on the theca interna layer.

SCARB1 was found in the cytoplasm of theca interna cells within all examined groups (Fig. 8A). However, the intensity of SCARB1-positive labeling was weaker in the VD group than in the C, I and VD + I groups ($p < 0.05$) (Fig. 8A'). Transmission electron microscopy ultrastructure analysis revealed the presence of LDs surrounded by mitochondria in theca interna cells (Fig. 8B). The mean number of LDs in theca interna cells was significantly lower in the VD group (2.87 ± 1.42 LDs per cell) than in the C group (8.70 ± 3.31 LDs per cell) and VD + I group (5.85 ± 3.25 LDs per cell) groups ($p < 0.05$). In addition, the lower numbers of LDs were observed in the I group (3.27 ± 2.09 LDs per cell) than in the C and VD + I groups ($p < 0.05$). Diminished LD accumulation was also noted in the VD + I group relative to the C group ($p < 0.05$) (Fig. 8B').

## 4. Discussion

The present study is the first to perform a global TMT-based proteomic analysis of the interactions between VD and I within the granulosa and theca interna compartments of the ovarian follicle using the pig as a model. We identified 97 DAPs in the granulosa layer and 11 DAPs within the theca interna layer, indicating a greater response of granulosa cells to the tested compounds. In granulosa cells, 44 DAPs were found in the comparison VD + I *vs* C, while in theca interna cells, 8 DAPs were found in the VD + I and C groups. These findings confirm the importance of VD and I cross-talk in both follicle layers. Importantly, most of these DAPs were related to cell cycle progression and proliferation in the granulosa layer, and cholesterol transport in the theca interna layer clearly showing the impact of VD and I interactions on crucial ovarian functions (namely folliculogenesis and steroidogenesis). However, novel molecular mechanisms underlying these processes have been proposed (Fig. 9).

As a dynamically changing structure, the ovarian follicle requires coordinated granulosa cell proliferation, not only for its growth but also for creating an optimal milieu for the oocyte maturation [2]. VD has been shown to be a positive regulator of granulosa cell proliferation in humans [38], goats [11,12], pigs [39], and hens [40], mainly *via* regulation of cell cycle-related factors such as cyclins, cyclin-dependent kinases, and their inhibitors. In pigs and goats, another proposed mechanism of granulosa cell proliferation involves a VD-induced decrease in the production of reactive oxygen species [11,39]. In accordance with these previous findings, we demonstrated increased proliferation of porcine granulosa cells in the VD group in comparison to the C group using a proliferation assay. To further confirm this effect, we applied flow cytometry and showed an increased percentage of S-phase cells. Similar results were reported for granulosa cells from pre-hierarchical follicles of hens [40] and the human granulosa KGN cell line [38]. These results suggest that VD promotes granulosa cell proliferation by inducing these cells to enter the S-phase, in which DNA synthesis occurs.

Unexpectedly, among the biological pathways overrepresented in a group of DAPs identified in the comparison VD *vs* C, none were associated with the cell cycle or proliferation. This prompted us to investigate whether any proteins up-regulated by VD could be involved in these processes. Among other proteins, calcium-binding protein S100A6 (S100A6) was found to increase cell proliferation through regulation of the cell cycle [41,42]. In hepatocellular carcinoma overexpression of S100A6 promoted cell proliferation and migration by enhanced degradation of p53, which is responsible for growth arrest [43]. In addition, diaphanous related formin 3 (DIAPH3) enhanced cell proliferation through the mTOR signaling pathway in cervical cancer [44], whereas myristoylated alanine-rich C-kinase substrate like 1 (MARCKSL1) stimulated proliferation of lung adenocarcinoma cells and decreased the expression of epithelial-mesenchymal transition-associated proteins through the RAC serine/threonine kinases (AKT) pathway [45]. The present study showed that increased abundance of S100A6, DIAPH3, and MARCKSL1 proteins may lead to VD-induced proliferation of porcine granulosa cells. However, these candidate proteins require further evaluation.

In this paper, we describe for the first time the enhanced proliferation of granulosa cells in the VD + I group relative to the C group, which is associated with a greater percentage of S-phase cells. This indicates a synergistic action of VD and I in promoting porcine granulosa cell proliferation through increased DNA replication. Consistent with these findings, an LC-MS/MS analysis revealed up-regulation of two core replisome components: DNA polymerase alpha catalytic subunit (POLA1), which plays an essential role in the initiation of DNA synthesis, and its direct partner, WD repeat and HMG-box DNA binding protein 1 (WDHD1) [46]. Interestingly, STRING analysis revealed strong PPIs between POLA1 and WDHD1 as well as other DAPs annotated to the cell cycle enrichment pathway. Among others, kinesin family member 11 (KIF11), TPX2 microtubule nucleation factor (TPX2) and nucleolar and spindle associated protein 1 (NUSAP1) are crucial for normal assembly and organization of mitotic spindles that begins upon mitotic entry [47–49], while anillin actin binding protein (ANLN) is required for the proper cytokinesis [50]. All these DAPs were up-regulated in the present study and could thereby facilitate granulosa cell cycle progression. In the VD + I group, we also noted the down-regulation of transcription factor jun-B (JUNB), which inhibits cell division. An earlier report indicated that JUNB accumulation led to cell cycle arrest in the G1 phase *via* induction of the cell cycle kinase inhibitor $p16^{INK4\alpha}$ [51]. Given that JUNB was previously detected in the nuclei of porcine granulosa cells [52], decreased abundance of JUNB as shown in the present study may additionally contribute to the induction of porcine granulosa cell proliferation following concomitant VD and I treatment. Given that I was shown to affect granulosa cell proliferation in PCOS *via* decreasing VDR expression [53], our present findings related to VD and I cross-talk appear to have a potential implication in the improvement of ovarian cell viability in PCOS and this possibility is worth further investigation.

The results of our in-depth proteomic analysis suggest that the molecular mechanisms underlying increased proliferation of granulosa cells in the VD and VD + I groups differ at the protein level. Notably, the most enriched pathways in the comparison VD *vs* VD + I were "cell cycle",

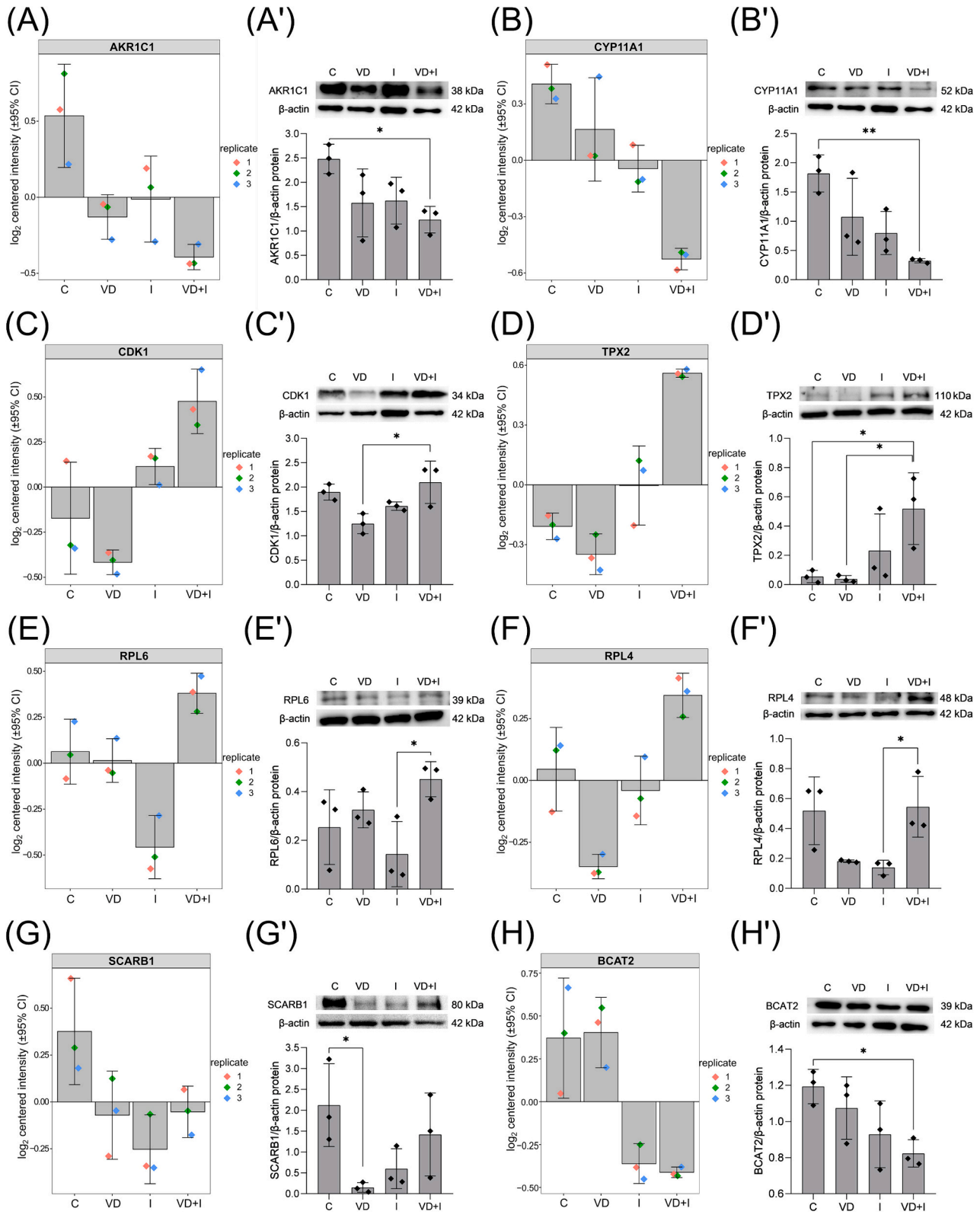


**Fig. 6.** Validation of proteomic results by Western blot analysis.
Western blot analysis was used to confirm the differentiated abundance of selected proteins: 6 proteins (AKR1C1, CYP11A1, CDK1, TPX2, RPL6, and RPL4) within the granulosa layer and 2 proteins (SCARB1 and BCAT2) within the theca interna layer of porcine ovarian follicles cultured *in vitro* from control (C), vitamin $D_3$ (VD), insulin (I), and both vitamin $D_3$ and insulin (VD + I) treated groups. **(A-H)** The graphs show the $\log_2$ centered intensity of selected proteins obtained from LC-MS/MS analysis using R software. **(A'-H')** The graphs show the relative protein abundance measured by densitometry and expressed as the ratio relative to β-actin as the endogenous control. Data are presented as mean ± standard deviation ($n = 3$). * $p < 0.05$, ** $p < 0.01$ (one-way ANOVA followed by Tukey's *post hoc* test). AKR1C1, aldo-keto reductase family 1 member C1; CYP11A1, cholesterol side-chain cleavage enzyme, mitochondrial; CDK1, cyclin-dependent kinase 1; TPX2, TPX2 microtubule nucleation factor; RPL6, 60S ribosomal protein L6; RPL4, 60S ribosomal protein L4; SCARB1, scavenger receptor class B member 1; BCAT2, branched-chain-amino-acid aminotransferase, mitochondrial.

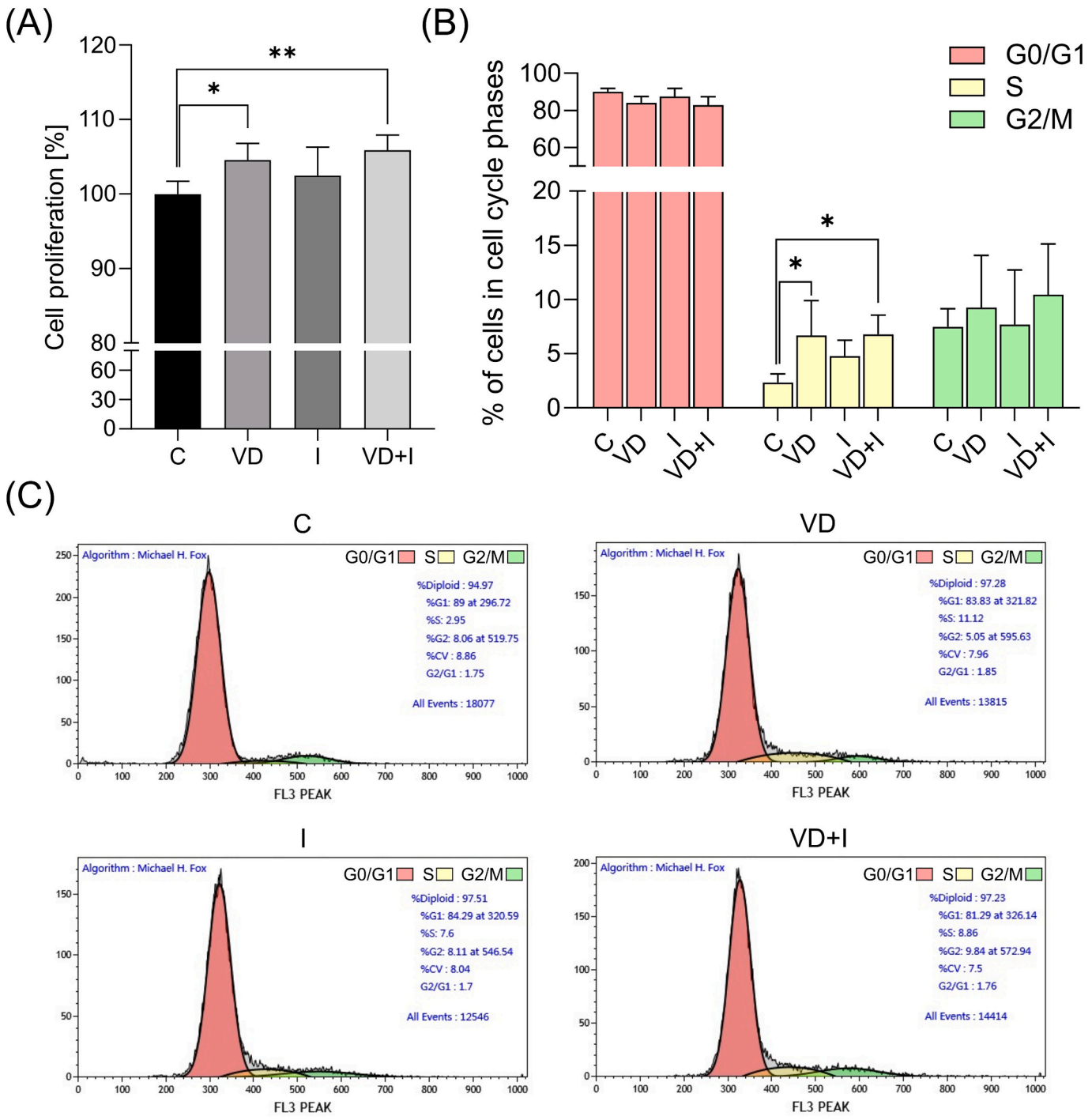


**Fig. 7.** Proliferation and cell cycle analysis of porcine granulosa cells cultured *in vitro* from control (C), vitamin $D_3$ (VD), insulin (I), and both vitamin $D_3$ and insulin (VD + I) treated groups.
**(A)** Effects of VD, I, and VD + I *in vitro* treatment on porcine granulosa cell proliferation. The Y-axis represents the percentage of proliferating cells. Data are presented as mean ± standard deviation (SD) ($n = 6$). * $p < 0.05$, ** $p < 0.01$ (one-way ANOVA followed by Tukey's *post hoc* test). **(B)** Effects of VD, I, and VD + I *in vitro* treatment on the distribution of cell cycle phases G0/G1, S and G2/M analyzed by flow cytometry. The Y-axis represents the percentage of cells in each phase. **(C)** Representative histograms of flow cytometry analysis of porcine granulosa cells following VD, I, and VD + I *in vitro* treatment. The Y-axis shows the number of cells counted, and the X-axis shows the fluorescence of propidium iodide. Data are presented as mean ± SD ($n = 4$). * $p < 0.05$ (one-way ANOVA followed by Tukey's *post hoc* test).

"microtubule cytoskeleton organization involved in mitosis", and "protein binding", and all DAPs associated with the cell cycle (KIF20 A, NCAPH, CENPF, DLGAP5, POLA1, NUF2, SPC24, TIMELESS, NUSAP1, CDK1, TPX2, PRC1, KIF11, ANLN, and FANCD2) and microtubule organization (DLGAP5, NUF2, NUSAP1, TPX2, PRC1, and KIF11) were down-regulated. Among them, kinesin family member 20 A (KIF20A) should be emphasized because of its crucial role in central spindle organization and cytokinesis. Furthermore, KIF20A is inhibited by cyclin-dependent kinase 1 (CDK1)-mediated phosphorylation, which ensures normal cell cycle progression [54]. KIF20A is commonly overexpressed in ovarian cancer, leading to enhanced cell proliferation [55]. In the present, KIF20A was also annotated to GO terms related to antral follicle

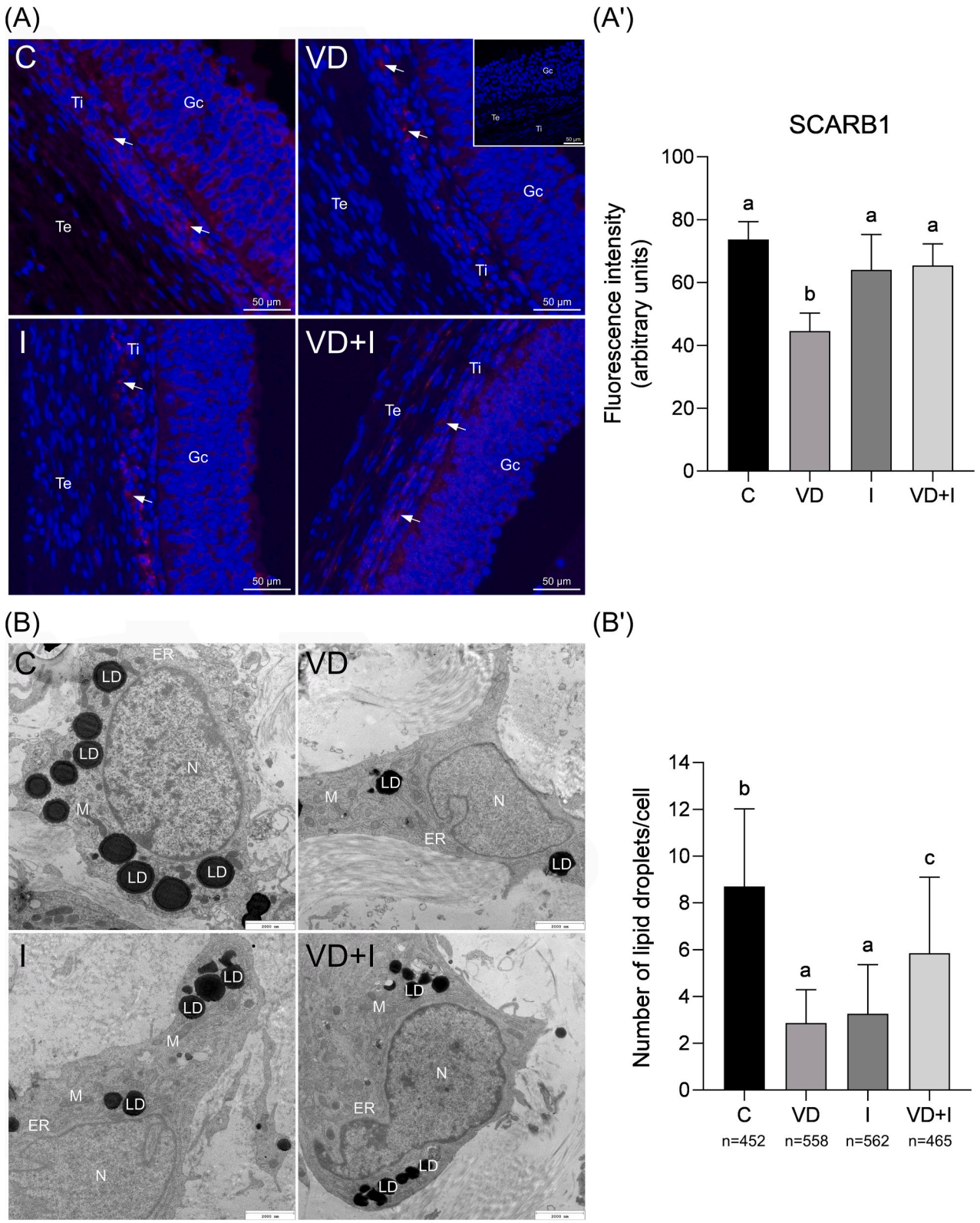


**Fig. 8.** **(A)** Immunofluorescent localization of scavenger receptor class B member 1 (SCARB1) and **(B)** transmission electron microscopy (TEM) analysis of lipid droplets in theca interna cells of porcine ovarian follicles cultured *in vitro* from control (C), vitamin $D_3$ (VD), insulin (I), and both vitamin $D_3$ and insulin (VD + I) treated groups. **(A)** Representative microphotographs of immunofluorescent staining for SCARB1 protein and **(A')** quantification of mean fluorescence intensity of SCARB1 in theca interna cells. Positive (red) labeling within the theca interna layer is marked by white arrows. DAPI staining (blue) affects the nuclei only. Negative control is shown in the inset of (A). **(B)** Representative TEM images of theca interna cells containing lipid droplets and **(B')** quantification of the number of lipid droplets per cell in each treatment group based on the number of cells indicated in the images (n, below X-axis). The graphs present the mean ± standard deviation. Different superscript letter indicate statistically significant differences ($p < 0.05$; one-way ANOVA followed by Tukey's *post hoc* test). ER, endoplasmic reticulum; Gc, granulosa cells; LD, lipid droplets; M, mitochondrion; N, nucleus; Ti, theca interna; Te, theca externa. (For interpretation of the references to colour in this figure legend, the reader is referred to the web version of this article.)

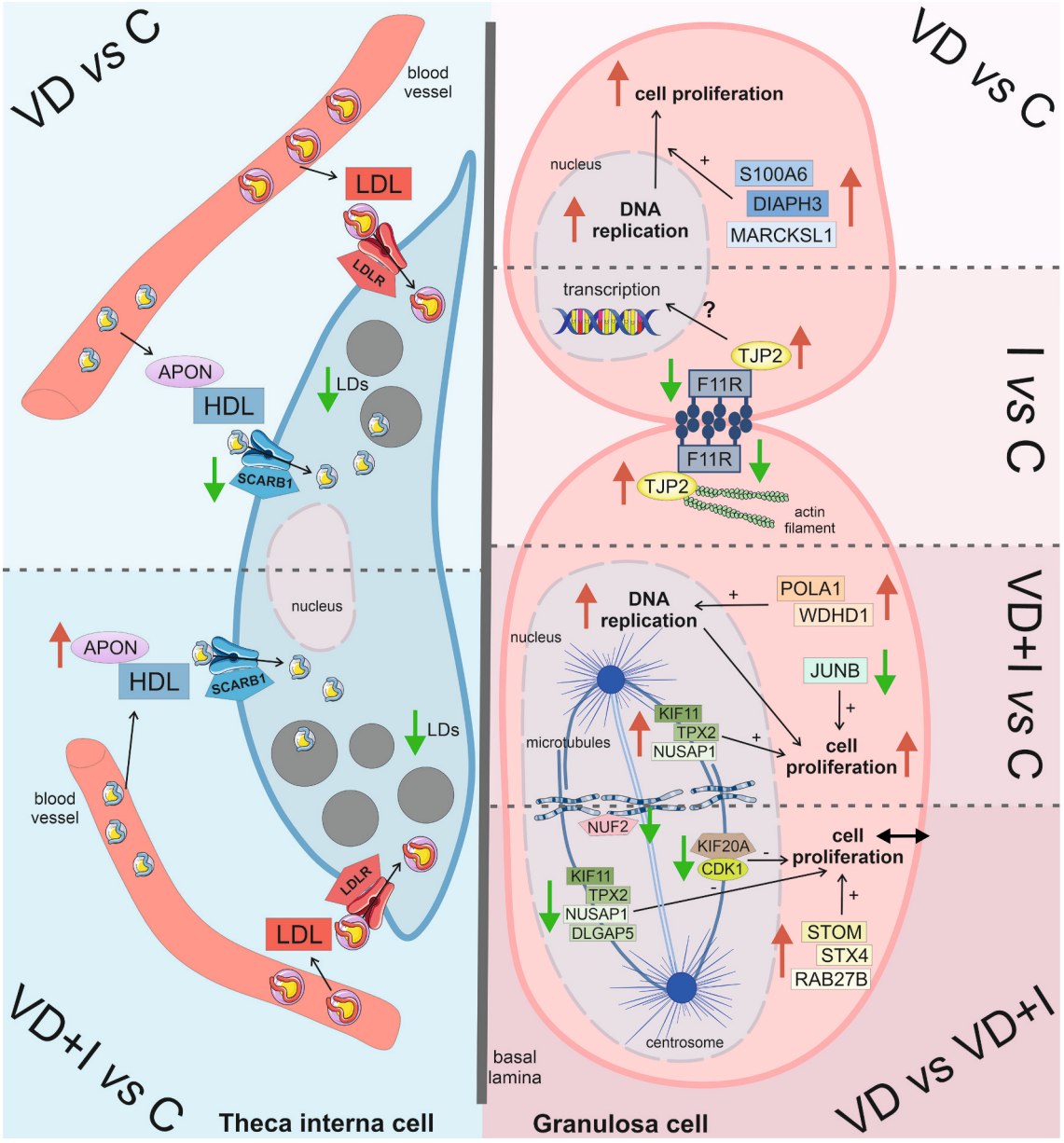


**Fig. 9.** Schematic representation illustrating the proposed mechanisms underlying the action of vitamin $D_3$ (VD) and insulin (I), alone or in combination (VD + I), in granulosa and theca interna cells of the porcine ovarian follicle.

In the granulosa layer, VD promotes cell proliferation presumably by enhanced DNA replication. It is also possible that increased abundance of S100A6, DIAPH3, and MARCKSL1 could be involved in granulosa cell proliferation. I influences tight junction proteins by down-regulating transmembrane F11R and up-regulating cytoplasmic TJP2, thus contributing to cellular adhesion and cell-cell communication. TJP2 is also considered a transcription factor. VD and I concomitantly induce porcine granulosa cell proliferation through increased DNA synthesis, which is stimulated by increased abundance of POLA1 and WDHD1. Furthermore, the up-regulation of KIF11, TPX2, and NUSAP1 involved in spindle assembly and the down-regulation of the cell cycle inhibitor JUNB may also contribute to granulosa cell proliferation. In the comparison VD *vs* VD + I, many proteins involved in the cell cycle (*e.g.* KIF20 A and CDK1), microtubule organization (*e.g.* DLGAP5, NUSAP1, TPX2, and KIF11) and chromosome segregation (*e.g.* NUF2) were down-regulated, whereas others recognized to promote cell proliferation (including STOM, STX4, and RAB27B) were up-regulated. Overall, this might result in unchanged granulosa cell proliferation.

In the theca interna layer, VD down-regulated the abundance of SCARB1 (a selective HDL receptor) potentially resulting in diminished LD accumulation. In the VD + I group, the abundance of SCARB1 was unchanged; however, the up-regulation of APON could be a compensatory mechanism increasing HDL-bound cholesterol transport to theca interna cells.

APON, apolipoprotein N; C, control; CDK1, cyclin dependent kinase 1; DIAPH3, diaphanous related formin 3; DLGAP5, DLG-associated protein 5; F11R, junctional adhesion molecule 1; HDL, high-density lipoproteins; I, insulin; JUNB, transcription factor jun-B; KIF11, kinesin family member 11; KIF20 A, kinesin family member 20 A; LDs, lipid droplets; LDL, low-density lipoprotein; LDLR, low-density lipoprotein receptor; MARCKSL1, myristoylated alanine-rich kinase C substrate like 1; NUF2, NUF2 component of NDC80 kinetochore complex; NUSAP1, nucleolar and spindle associated protein 1; POLA1, DNA polymerase; RAB27B, small monomeric GTPase; S100A6, protein S100-A6; SCARB1, scavenger receptor class B member 1; STOM, stomatin; STX4, syntaxin 4; TJP2, tight junction protein 2; TPX2, TPX2 microtubule nucleation factor; VD, vitamin $D_3$; WDHD1, WD repeat and HMG-box DNA binding protein 1; red ↑, up-regulation; green ↓, down-regulation; black ↔, unchanged; +, stimulation; −, inhibition. (For interpretation of the references to colour in this figure legend, the reader is referred to the web version of this article.)

growth and oocyte maturation, highlighting its crucial role in regulation of female reproductive processes. Indeed, KIF20A has been demonstrated to be essential for extrusion of the first polar body in the oocytes of mice [56] and pigs [57]. The lack of differences in cell cycle progression between the VD and VD + I groups in the present study despite decreased abundance of cell cycle-related proteins may be partly explained by the up-regulation of DAPs that promote cell proliferation, including stomatin (STOM) [58], syntaxin 4 (STX4) [59], and small monomeric GTPase (RAB27B) [60]. Fundamental to the current understanding of the underlying mechanism could be the functional PPIs disclosed by STRING analysis between up-regulated and down-regulated DAPs associated with the cell cycle: STOM and CDK1, as well as STX4 and centromere protein F (CENPF).

The proliferation, differentiation, and proper functioning of granulosa cells require mutual communication ensured by adhesive molecules of TJs, adherens junctions, and desmosomes [61]. Adherens junctions and desmosomes predominantly provide the adhesion between cells, while TJs control the paracellular transport of water, ions, and macromolecules [62]. In the comparison I *vs* C within the granulosa layer in the present study, we noted strong PPIs between two TJ components: the down-regulated transmembrane junctional adhesion molecule 1 (F11R) and the up-regulated cytoplasmic scaffolding tight junction protein 2 (TJP2). In previous research, F11R and TJP2 were detected in the granulosa cells of mouse ovarian follicles with a notable reduction in the abundance of F11R protein within follicle growth [62]. Additionally, the mRNA transcript abundance of other TJ proteins, such as occludin, tight junction protein 1, and cingulin, decreased during development of bovine antral follicles [63]. This suggests that the down-regulation of TJ proteins can reduce barrier function, thereby increasing the volume of follicular fluid [63]. Along these lines, the insulin-induced decrease in F11R protein abundance observed in granulosa cells may result in enlargement of the porcine follicle size and this could be important in the context of hyperinsulinemia and ovarian cysts accompanying PCOS [17]. The dysregulation of F11R expression may also promote cell apoptosis as reported in various types of cancer, including lung adenocarcinoma and breast cancer [64]. Moreover, several lines of evidence have suggested that overexpression of TJP2 protein participates in signal transduction pathways leading to apoptosis [65,66] because of its role in nuclear signaling [67]. We recently observed increased apoptosis of granulosa cells following insulin treatment using the same model of whole porcine ovarian follicle incubation [25]. The observed results, namely the decrease in F11R abundance and increase in TJP2 abundances within the granulosa layer, may be associated with the induction of apoptosis and explain, in part, a molecular mechanism of this event. However, a recent study revealed similar abundance of F11R and TJP2 in the VD + I group with simultaneous lack of apoptosis induction [25]. This may indicate that both compounds together promote expression of proteins that stimulate granulosa cell proliferation, as described above.

The vital role of the ovarian follicle is steroid hormone biosynthesis. This process requires collaboration between granulosa cells (which produce estrogens) and adjacent theca interna cells (which provide their immediate precursors, *i.e.* androgens) [2]. The onset of steroidogenesis involves the uptake of cholesterol, which is predominantly stored as cholesterol esters in LDs or associated with plasma low-density lipoproteins (LDLs) and high-density lipoproteins (HDLs) [68]. Theca cells are directly accessible to both types of cholesterol-bound lipoproteins [3]. Among the DAPs identified in the theca interna layer, we found the scavenger receptor class B member 1 (SCARB1), a selective HDL receptor that mediates HDL accumulation in LDs [69]. The LC-MS/MS and Western blot analyses showed that the abundance of SCARB1 protein was down-regulated in the VD group relative to the C group. This was additionally confirmed by decreased SCARB1 immunofluorescence intensity within theca interna cells. Our present findings suggest attenuated HDL transport *via* SCARB1 into theca interna cells of porcine ovarian follicles, leading to diminished intracellular cholesterol accumulation. Indeed, we also observed reduced number of LDs following VD treatment, which might further impact the steroidogenesis in the theca interna compartment. Notably, deficiency of SCARB1 negatively affects progesterone production in human granulosa cells [70] and mice luteal tissue [71]. However, the mechanisms underlying VD-regulated cholesterol transport within ovarian cells, including theca cells, has not been investigated. Considering that VD supplementation lowers the total testosterone and androstenedione levels in women with PCOS, which are overproduced by the theca interna layer [72], and considering the recently reported association of *SCARB1* variants with PCOS [73], a potential effect of VD on theca interna steroidogenesis through SCARB1-mediated cholesterol transport cannot be ruled out and is worthy deeper investigation. Such research represents another step toward developing a feasible treatment for PCOS.

Among the DAPs revealed in the theca interna layer, we also identified apolipoprotein N (APON), which showed increased abundance in the VD + I group relative to the C group. Apolipoproteins are protein components of lipoproteins, which facilitate the transport of lipids. Apolipoprotein E (APOE) has been implicated in cholesterol delivery within ovarian follicles, either by participating in the lipoprotein–receptor complex or lipid endocytosis, to regulate steroidogenesis [74]. In previous research, APOE transcript and protein were found in the theca and interstitial cells of mice [75], and its paracrine effect on androgen synthesis was dose-dependent; specifically, APOE inhibited androgen production at high concentrations and stimulated androgen production at low concentrations [76]. Although APON was detected in the current study, its precise role in the mammalian ovary remains unknown. APON has been identified in the HDL and LDL fractions of bovine follicular fluid and in the HDL fraction of bovine serum, and it has been shown to be immunolocalized in both granulosa and theca cells [77]. Based on outcomes from research on APOE [74] and the molecular characteristics of APON [77], the involvement of APON in cholesterol uptake and further androgens synthesis within the theca interna layer seems plausible. In the present study, considering that LD accumulation in the theca interna cells was greater in the VD + I group than in the VD group with no change in SCARB1 abundance, the up-regulation of APON after VD + I treatment could be a compensatory mechanism increasing HDL-bound cholesterol transport to the theca interna layer. Overall, this TMT-based proteomic analysis of the porcine theca interna layer has revealed for the first that VD alone or in co-treatment with I can influence HDL-associated cholesterol uptake and, in turn, further steroidogenesis. However, the underlying mechanism appears to differ between the two treatment regiments.

Although our study provides promising new insights into the proteomic interactions of VD and I within the ovarian follicle, our study does have potential limitations. First, the experiment was performed on the whole porcine antral follicle, which was used as a physiological model reflecting complex biological cross-talk between granulosa and theca cells. However, this model allowed us to conduct *in vitro* incubation for no longer than 12 h, thereby avoiding follicular degeneration as we recently described [25]. Accordingly, there is plausible that only the most pronounced DAPs were revealed and less differentiated proteins were not detected. Second, our study was based on commonly used doses of VD and I, indicating a set of DAPs, but it does not rule out the possibility that different DAPs are identified at different doses. However, the usage of common VD and I doses enables the comparison of protein expression pattern across different species, including human. Third, the number of identified DAPs depends on the arbitrarily chosen parameters of bioinformatic analysis, such as FC cut-off. In this study, the FC was set up as 1.5 to filter out DAPs with small changes. Noteworthy, the public deposition of proteomics data provides the possibility of their reanalysis with alternative settings. At the end, we applied herein antibody-based methods, including Western blot and immunofluorescence, for the proteomics data validation. Quantitative mass spectrometry data validation by a semi-quantitative Western blot becomes a moot point in the scientific community due its lower specificity and reproducibility

[78,79]. However from the biologist's viewpoint it is useful if applied to confirm the abundance of proteins involved in particular biological processes revealed by the quantitative proteomic data as presented in this study. In addition, we posit that the use of alternative antibody-based methods of validation, such as immunofluorescence staining, may be suitable in the context of protein distribution in the cell.

There is a close genetic and proteomic similarities between pigs and humans, thus the study of pig proteomics datasets is crucial for advancing human biomedical research and it is an urgent need for the systematic creation of proteome catalogs for different porcine tissues [23,80]. The identification of DAPs involved in the cross-talk between VD and I in the ovarian follicle appears to be valuable in the field of reproductive biology, and would be useful to better understand VD role in counteracting hyperinsulinemia at the ovary level.

Collectively, this paper is the first to describe the effects of VD and I on the global proteomic profile of granulosa and theca interna cells of the porcine ovarian follicle, revealing specific molecular hallmarks that may serve as useful biomarkers of the interactions occurring between them in both follicle layers. In the granulosa cells, VD affected proteome (*e.g.* S100A6, DIAPH3, and MARCKSL1) leading to the promotion of cell proliferation, whereas I influenced mainly proteins related to cellular adhesion (*e.g.* F11R and TJP2). The VD + I treatment induced granulosa cell proliferation probably *via* the DAPs involved in DNA synthesis and the cell cycle regulation (*e.g.* KIF11, TPX2, NUSAP1, JUNB, POLA1, and WDHD1). In the theca interna layer, VD alone or in co-treatment with I affected DAPs associated with cholesterol transport (*e.g.* SCARB1 and APON) that was further confirmed by diminished LDs accumulation (Fig. 9). Interestingly, several identified DAPs have also been described in relation to PCOS, including SCARB1 [73], KIF11 [81], and F11R [82]. These findings provide a framework for further research on the mechanism of VD and I action in the ovary as well as possible implications in relation to ovarian diseases characterized by impaired VD and I levels, such as PCOS.

## Funding

Funding for this study was provided by the National Science Center, Poland (PRELUDIUM BIS 1 project no. 2019/35/O/NZ9/02678 to MG) and partly by the Programme "Excellence Initiative-Research University" at the Jagiellonian University in Krakow, Poland (no. U1U/W18/NO/28.41 to KK).

## CRediT authorship contribution statement

**Kinga Kamińska:** Visualization, Validation, Methodology, Investigation, Funding acquisition, Formal analysis, Conceptualization, Writing – original draft. **Bianka Świderska:** Methodology, Investigation. **Agata Malinowska:** Formal analysis. **Małgorzata Grzesiak:** Supervision, Resources, Project administration, Funding acquisition, Formal analysis, Conceptualization, Writing – review & editing, Writing – original draft.

## Declaration of competing interest

The authors declare no conflicts of interest.

## Data availability

The mass spectrometry proteomics data have been deposited to the ProteomeXchange Consortium via the PRIDE [83] partner repository with the dataset identifier PXD050533 and 10.6019/PXD050533. Other data are available in Rodbuk UJ or on request from the corresponding author.

## Acknowledgments

The authors would like to thank the Department of Cell Biology and Imaging of the Institute of Zoology and Biomedical Research, the Jagiellonian University, Kraków, Poland for the access to the transmission electron microscope (JEOL JEM 2100HT) and Malopolska Centre of Biotechnology, the Jagiellonian University, Kraków, Poland for the access to the flow cytometry (CytoFLEX flow cytometer).

## Appendix A. Supplementary data

Supplementary data to this article can be found online at https://doi.org/10.1016/j.jprot.2024.105318.

## References

[1] M.A. Edson, A.K. Nagaraja, M.M. Matzuk, The mammalian ovary from genesis to revelation, Endocr. Rev. 30 (2009) 624–712, https://doi.org/10.1210/er.2009-0012.
[2] J.F. Strauss, C.J. Williams, Chapter 8 - Ovarian life cycle, in: J.F. Strauss, R. L. Barbieri (Eds.), Yen and Jaffe's Reproductive Endocrinology (Eighth Edition), Elsevier, 2019, 167–205.e9.
[3] J.M. Young, A.S. McNeilly, Theca: the forgotten cell of the ovarian follicle, Reproduction 140 (2010) 489–504, https://doi.org/10.1530/REP-10-0094.
[4] N. Rimon-Dahari, L. Yerushalmi-Heinemann, L. Alyagor, N. Dekel, Ovarian folliculogenesis, Results Probl. Cell Differ. 58 (2016) 167–190, https://doi.org/10.1007/978-3-319-31973-5_7.
[5] M. Grzesiak, Vitamin $D_3$ action within the ovary - an updated review, Physiol. Res. 69 (2020) 371–378, https://doi.org/10.33549/physiolres.934266.
[6] F. Xu, S. Wolf, O. Green, J. Xu, Vitamin D in follicular development and oocyte maturation, Reproduction 161 (2021) R129–R137, https://doi.org/10.1530/REP-20-0608.
[7] M. Grzesiak, M. Tchurzyk, M. Socha, A. Sechman, A. Hrabia, An overview of the current known and unknown roles of vitamin $D_3$ in the female reproductive system: lessons from farm animals, birds, and fish, Int. J. Mol. Sci. 23 (2022) 14137, https://doi.org/10.3390/ijms232214137.
[8] J. Xu, M.S. Lawson, F. XuF, et al., Vitamin $D_3$ regulates follicular development and intrafollicular vitamin D biosynthesis and signaling in the primate ovary, Front. Physiol. 9 (2018), https://doi.org/10.3389/fphys.2018.01600, 1600.
[9] M. Grzesiak, K. Knapczyk-Stwora, M. Slomczynska, Vitamin $D_3$ in ovarian antral follicles of mature gilts: expression of its receptors and metabolic enzymes, concentration in follicular fluid and effect on steroid secretion *in vitro*, Theriogenology 160 (2021) 151–160, https://doi.org/10.1016/j.theriogenology.2020.11.006.
[10] J. Xu, J.D. Hennebold, D.B. Seifer, Direct vitamin $D_3$ actions on rhesus macaque follicles in three-dimensional culture: assessment of follicle survival, growth, steroid, and anti-müllerian hormone production, Fertil. Steril. 106 (2016) 1815–1820, https://doi.org/10.1016/j.fertnstert.2016.08.037.
[11] X. Yao, G. Zhang, Y. Guo, et al., Vitamin D receptor expression and potential role of vitamin D on cell proliferation and steroidogenesis in goat ovarian granulosa cells, Theriogenology 102 (2017) 162–173, https://doi.org/10.1016/j.theriogenology.2017.08.002.
[12] X. Yao, Z. Wang, M.A. El-Samahy, et al., Roles of vitamin D and its receptor in the proliferation and apoptosis of luteinised granulosa cells in the goat, Reprod. Fertil. Dev. 32 (2020) 335–348, https://doi.org/10.1071/RD18442.
[13] Z.O. Merhi, D.B. Seifer, J. Weedon, et al., Circulating vitamin D correlates with serum antimüllerian hormone levels in late-reproductive-aged women: Women's interagency HIV study, Fertil. Steril. 98 (2012) 228–234, https://doi.org/10.1016/j.fertnstert.2012.03.029.
[14] Z. Merhi, A. Doswell, K. Krebs, M. Cipolla, Vitamin D alters genes involved in follicular development and steroidogenesis in human cumulus granulosa cells, J. Clin. Endocrinol. Metab. 99 (2014) E1137–E1145, https://doi.org/10.1210/jc.2013-4161.
[15] K. Kaminska, M. Grzesiak, The relationship between vitamin $D_3$ and insulin in polycystic ovary syndrome - a critical review, J. Physiol. Pharmacol. 72 (2021) 13–22, https://doi.org/10.26402/jpp.2021.1.02.
[16] G. Morgante, I. Darino, A. Spanò, et al., PCOS physiopathology and vitamin D deficiency: biological insights and perspectives for treatment, J. Clin. Med. 11 (2022) 4509, https://doi.org/10.3390/jcm11154509.
[17] S. Chang, A. Dunaif, Diagnosis of polycystic ovary syndrome: which criteria to use and when? Endocrinol. Metab. Clin. N. Am. 50 (2021) 11–23, https://doi.org/10.1016/j.ecl.2020.10.002.
[18] P. Moghetti, F. Tosi, Insulin resistance and PCOS: chicken or egg? J. Endocrinol. Investig. 44 (2021) 233–244, https://doi.org/10.1007/s40618-020-01351-0.
[19] J. Dupont, R.J. Scaramuzzi, Insulin signalling and glucose transport in the ovary and ovarian function during the ovarian cycle, Biochem. J. 473 (2016) 1483–1501, https://doi.org/10.1042/BCJ20160124.
[20] H. Zhao, J. Zhang, X. Cheng, X. Nie, B. He, Insulin resistance in polycystic ovary syndrome across various tissues: an updated review of pathogenesis, evaluation, and treatment, J. Ovarian Res. 16 (2023) 9, https://doi.org/10.1186/s13048-022-01091-0.

[21] R. Kalyanaraman, L. Pal, A narrative review of current understanding of the pathophysiology of polycystic ovary syndrome: focus on plausible relevance of vitamin D, Int. J. Mol. Sci. 22 (2021) 4905, https://doi.org/10.3390/ijms22094905.
[22] K.N. Kuzmuk, L.B. Schook, Pig as a model for biomedical sciences, in: M. F. Rothschild, A. Ruvinsky (Eds.), The Genetics of the Pig, CABI Publishing, 2011, pp. 426–444.
[23] N. Verma, A.W. Rettenmeier, S. Schmitz-Spanke, Recent advances in the use of *Sus scrofa* (pig) as a model system for proteomic studies, Proteomics 11 (2011) 776–793, https://doi.org/10.1002/pmic.201000320.
[24] E.L. Akins, M.C. Morrissette, Gross ovarian changes during estrous cycle of swine, Am. J. Vet. Res. 29 (1968) 1953–1957.
[25] K. Kamińska, E. Wiercigroch, K. Małek, M. Grzesiak, Biomolecular composition of porcine ovarian follicles following in vitro treatment of vitamin $D_3$ and insulin alone or in combination, Reprod. Biol. 23 (2023) 100818, https://doi.org/10.1016/j.repbio.2023.100818.
[26] K. Smolikova, A. Mlynarcikova, S. Scsukova, Effect of 1α,25-dihydroxyvitamin $D_3$ on progesterone secretion by porcine ovarian granulosa cells, Endocr. Regul. 47 (2013) 123–131, https://doi.org/10.4149/endo_2013_03_123.
[27] S. Rice, L.J. Pellatt, S.J. Bryan, S.A. Whitehead, H.D. Mason, Action of metformin on the insulin-signaling pathway and on glucose transport in human granulosa cells, J. Clin. Endocrinol. Metab. 96 (2011) E427–E435, https://doi.org/10.1210/jc.2010-2060.
[28] S. Stoklosowa, E. Gregoraszczuk, C.P. Channing, Estrogen and progesterone secretion by isolated cultured porcine thecal and granulosa cells, Biol. Reprod. 26 (1982) 943–952, https://doi.org/10.1095/biolreprod26.5.943.
[29] J.R. Wiśniewski, A. Zougman, N. Nagaraj, M. Mann, Universal sample preparation method for proteome analysis, Nat. Methods 6 (5) (2009) 359–362, https://doi.org/10.1038/nmeth.1322.
[30] E. Ziemlińska, J. Sobocińska, A. Świątkowska, et al., Palm oil-rich diet affects murine liver proteome and S-palmitoylome, Int. J. Mol. Sci. 22 (2021) 13094, https://doi.org/10.3390/ijms222313094.
[31] I. Jancewicz, J. Szarkowska, R. Konopinski, et al., PD-L1 overexpression, SWI/SNF complex deregulation, and profound transcriptomic changes characterize cancer-dependent exhaustion of persistently activated CD4+ T cells, Cancers (Basel) 13 (2021) 4148, https://doi.org/10.3390/cancers13164148.
[32] S. Tyanova, T. Temu, J. Cox, The MaxQuant computational platform for mass spectrometry-based shotgun proteomics, Nat. Protoc. 11 (2016) 2301–2319, https://doi.org/10.1038/nprot.2016.136.
[33] S. Yoon, B. Baik, T. Park, D. Nam, Powerful p-value combination methods to detect incomplete association, Sci. Rep. 11 (2021) 6980, https://doi.org/10.1038/s41598-021-86465-y.
[34] J. Piibor, A. Waldmann, K. Dissanayake, et al., Uterine fluid extracellular vesicles proteome is altered during the estrous cycle, Mol. Cell. Proteomics 11 (2023) 100642, https://doi.org/10.1016/j.mcpro.2023.100642.
[35] L. Kolberg, U. Raudvere, I. Kuzmin, P. Adler, J. Vilo, H. Peterson, g:Profiler-interoperable web service for functional enrichment analysis and gene identifier mapping (2023 update), Nucleic Acids Res. 51 (2023) W207–W212, https://doi.org/10.1093/nar/gkad347.
[36] D. Szklarczyk, R. Kirsch, M. Koutrouli, et al., The STRING database in 2023: Protein-protein association networks and functional enrichment analyses for any sequenced genome of interest, Nucleic Acids Res. 51 (2023) D638–D646, https://doi.org/10.1093/nar/gkac1000.
[37] M.H. Shihan, S.G. Novo, S.J. Le Marchand, Y. Wang, M.K. Duncan, A simple method for quantitating confocal fluorescent images, Biochem. Biophys. Rep. 25 (2021) 100916, https://doi.org/10.1016/j.bbrep.2021.100916.
[38] R. Hu, L. Li, L. Liang, Y. Qi, X. Ma, Y. Yang, 25(OH)$D_3$ improves granulosa cell proliferation and IVF pregnancy outcomes in patients with endometriosis by increasing G2M+S phase cells, Reprod. Biol. Endocrinol. 21 (2023) 115, https://doi.org/10.1186/s12958-023-01165-8.
[39] S. Wang, Q. Yao, F. Zhao, et al., 1α,25$(OH)_2D_3$ promotes the autophagy of porcine ovarian granulosa cells as a protective mechanism against ROS through the BNIP3/PINK1 pathway, Int. J. Mol. Sci. 24 (2023) 4364, https://doi.org/10.3390/ijms24054364.
[40] M. Cheng, Z. Song, Y. Guo, et al., 1α,25-dihydroxyvitamin $D_3$ improves follicular development and steroid hormone biosynthesis by regulating vitamin D receptor in the layers model, Curr. Issues Mol. Biol. 45 (2023) 4017–4034, https://doi.org/10.3390/cimb45050256.
[41] E.C. Breen, K. Tang, Calcyclin (S100A6) regulates pulmonary fibroblast proliferation, morphology, and cytosleletal organization in vitro, J. Cell. Biochem. 88 (2003) 848–854, https://doi.org/10.1002/jcb.10398.
[42] Y. Wang, X. Kang, X. Kang, F. Yang, S100A6: molecular function and biomarker role, Biomark. Res. 11 (2023) 78, https://doi.org/10.1186/s40364-023-00515-3.
[43] D. Song, B. Xu, D. Shi, S. Li, Y. Cai, S100A6 promotes proliferation and migration of HepG2 cells via increased ubiquitin-dependent degradation of p53, Open Med. (Wars) 15 (2020) 317–326, https://doi.org/10.1515/med-2020-0101.
[44] L. Wan, J. Zhu, Q. Wu, Knockdown of DIAPH3 inhibits the proliferation of cervical cancer cells through inactivating mTOR signaling pathway, J. Oncol. 2021 (2021) 4228241, https://doi.org/10.1155/2021/4228241.
[45] W. Liang, R. Gao, M. Yang, et al., MARCKSL1 promotes the proliferation, migration and invasion of lung adenocarcinoma cells, Oncol. Lett. 19 (2020) 2272–2280, https://doi.org/10.3892/ol.2020.11313.
[46] A.C. Simon, J.C. Zhou, R.L. Perera, et al., A Ctf4 trimer couples the CMG helicase to DNA polymerase α in the eukaryotic replisome, Nature 510 (7504) (2014) 293–297, https://doi.org/10.1038/nature13234.
[47] W.X. Yu, Y.K. Li, M.F. Xu, et al., Kinesin-5 Eg5 is essential for spindle assembly, chromosome stability and organogenesis in development, Cell Death Dis. 8 (2022) 490, https://doi.org/10.1038/s41420-022-01281-1.
[48] M.S. Safari, M.R. King, C.P. Brangwynne, S. Petry, Interaction of spindle assembly factor TPX2 with importins-α/β inhibits protein phase separation, J. Biol. Chem. 297 (2021) 100998, https://doi.org/10.1016/j.jbc.2021.100998.
[49] K. Ribbeck, T. Raemaekers, G. Carmeliet, I.W. Mattaj, A role for NuSAP in linking microtubules to mitotic chromosomes, Curr. Biol. 17 (2007) 230–236, https://doi.org/10.1016/j.cub.2006.11.050.
[50] W.M. Zhao, G. Fang, Anillin is a substrate of anaphase-promoting complex/cyclosome (APC/C) that controls spatial contractility of myosin during late cytokinesis, J. Biol. Chem. 280 (2005) 33516–33524, https://doi.org/10.1074/jbc.M504657200.
[51] E. Passegué, E.F. Wagner, JunB suppresses cell proliferation by transcriptional activation of p16(INK4a) expression, EMBO J. 19 (2000) 2969–2979, https://doi.org/10.1093/emboj/19.12.2969.
[52] R. Rusovici, H.A. LaVoie, Expression and distribution of AP-1 transcription factors in the porcine ovary, Biol. Reprod. 69 (2003) 64–74, https://doi.org/10.1095/biolreprod.102.013995.
[53] F. Kong, C. Du, Y. Wang, MicroRNA-9 affects isolated ovarian granulosa cells proliferation and apoptosis via targeting vitamin D receptor, Mol. Cell. Endocrinol. 486 (2019) 18–24, https://doi.org/10.1016/j.mce.2019.02.012.
[54] W.D. Wu, K.W. Yu, N. Zhong, Y. Xiao, Z.Y. She, Roles and mechanisms of Kinesin-6 KIF20A in spindle organization during cell division, Eur. J. Cell Biol. 98 (2019) 74–80, https://doi.org/10.1016/j.ejcb.2018.12.002.
[55] Y. Li, H. Guo, Z. Wang, et al., Cyclin F and KIF20A, FOXM1 target genes, increase proliferation and invasion of ovarian cancer cells, Exp. Cell Res. 395 (2020) 112212, https://doi.org/10.1016/j.yexcr.2020.112212.
[56] J. Liu, Q.C. Wang, X.S. Cui, Z.B. Wang, N.H. Kim, S.C. Sun, MKlp2 inhibitor paprotrain affects polar body extrusion during mouse oocyte maturation, Reprod. Biol. Endocrinol. 11 (2013) 117, https://doi.org/10.1186/1477-7827-11-117.
[57] Y. Zhang, J. Liu, X. Peng, et al., KIF20A regulates porcine oocyte maturation and early embryo development, PLoS One 9 (2014) e102898, https://doi.org/10.1371/journal.pone.0102898.
[58] R. Nadimpalli, N. Yalpani, G.S. Johal, C.R. Simmons, Prohibitins, stomatins, and plant disease response genes compose a protein superfamily that controls cell proliferation, ion channel regulation, and death, J. Biol. Chem. 275 (2000) 29579–29586, https://doi.org/10.1074/jbc.M002339200.
[59] K. Zeng, Q. Li, X. Wang, et al., STX4 as a potential biomarker for predicting prognosis and guiding clinical treatment decisions in clear cell renal cell carcinoma, Heliyon 10 (2023) e23918, https://doi.org/10.1016/j.heliyon.2023.e23918.
[60] Z. Li, R. Fang, J. Fang, S. He, T. Liu, Functional implications of Rab27 GTPases in cancer, Cell Commun. Signal 16 (2018) 44, https://doi.org/10.1186/s12964-018-0255-9.
[61] L. Zhang, T. Feng, L.J. Spicer, The role of tight junction proteins in ovarian follicular development and ovarian cancer, Reproduction 155 (2018) R183–R198, https://doi.org/10.1530/REP-17-0503.
[62] J.M. Mora, M.A. Fenwick, L. Castle, et al., Characterization and significance of adhesion and junction-related proteins in mouse ovarian follicles, Biol. Reprod. 86 (2012), https://doi.org/10.1095/biolreprod.111.096156, 153–14.
[63] L. Zhang, L.F. Schütz, C.L. Robinson, M.L. Totty, L.J. Spicer, Evidence that gene expression of ovarian follicular tight junction proteins is regulated *in vivo* and *in vitro* in cattle, J. Anim. Sci. 95 (2017) 1313–1324, https://doi.org/10.2527/jas.2016.0892.
[64] A. Lauko, Z. Mu, D.H. Gutmann, U.P. Naik, J.D. Lathia, Junctional adhesion molecules in cancer: a paradigm for the diverse functions of cell-cell interactions in tumor progression, Cancer Res. 80 (2020) 4878–4885, https://doi.org/10.1158/0008-5472.CAN-20-1829.
[65] T. Walsh, S.B. Pierce, D.R. Lenz, et al., Genomic duplication and overexpression of TJP2/ZO-2 leads to altered expression of apoptosis genes in progressive nonsyndromic hearing loss DFNA51, Am. J. Hum. Genet. 87 (2010) 101–109, https://doi.org/10.1016/j.ajhg.2010.05.011.
[66] W. Yang, Z. Zhang, L. Li, et al., ZNF582 overexpression restrains the progression of clear cell renal cell carcinoma by enhancing the binding of TJP2 and ERK2 and inhibiting ERK2 phosphorylation, Cell Death Dis. 14 (2023) 212, https://doi.org/10.1038/s41419-023-05750-y.
[67] H. Bauer, J. Zweimueller-Mayer, P. Steinbacher, A. Lametschwandtner, H.C. Bauer, The dual role of zonula occludens (ZO) proteins, J. Biomed. Biotechnol. 2010 (2010) 402593, https://doi.org/10.1155/2010/402593.
[68] W.L. Miller, H.S. Bose, Early steps in steroidogenesis: intracellular cholesterol trafficking, J. Lipid Res. 52 (2011) 2111–2135, https://doi.org/10.1194/jlr.R016675.
[69] S. Acton, A. Rigotti, K.T. Landschulz, et al., Identification of scavenger receptor SR-BI as a high density lipoprotein receptor, Science 271 (1996) 518–520, https://doi.org/10.1126/science.271.5248.518.
[70] A. Kolmakova, J. Wang, R. Brogan, C. Chaffin, A. Rodriguez, Deficiency of scavenger receptor class B type I negatively affects progesterone secretion in human granulosa cells, Endocrinology 151 (2010) 5519–5527, https://doi.org/10.1210/en.2010-0347.
[71] L.M. Jimenez, M. Binelli, K. Bertolin, R.M. Pelletier, B.D. Murphy, Scavenger receptor-B1 and luteal function in mice, J. Lipid Res. 51 (2010) 2362–2371, https://doi.org/10.1194/jlr.M006973.
[72] L. Pal, A. Berry, L. Coraluzzi, et al., Therapeutic implications of vitamin D and calcium in overweight women with polycystic ovary syndrome, Gynecol.

Endocrinol. 28 (2012) 965–968, https://doi.org/10.3109/09513590.2012.696753.
[73] D.M. Janani, S. Ramasubramanyan, V. Chellappa, et al., Whole exome and targeted sequencing reveal novel mutations associated with inherited PCOS condition in an Indian cohort, J. Hum. Genet. 68 (2023) 39–46, https://doi.org/10.1038/s10038-022-01093-2.
[74] R.B. Oriá, J.Z. de Almeida, C.N. Moreira, R.L. Guerrant, J.R. Figueiredo, Apolipoprotein E effects on mammalian ovarian steroidogenesis and human fertility, Trends Endocrinol. Metab. 31 (2020) 872–883, https://doi.org/10.1016/j.tem.2020.06.003.
[75] M. Nicosia, W.H. Moger, C.A. Dyer, M.M. Prack, D.L. Williams, Apolipoprotein-E messenger RNA in rat ovary is expressed in theca and interstitial cells and presumptive macrophage, but not in granulosa cells, Mol. Endocrinol. 6 (1992) 978–988, https://doi.org/10.1210/mend.6.6.1495495.
[76] C.V. Zerbinatti, L.P. Mayer, R.G. Audet, C.A. Dyer, Apolipoprotein E is a putative autocrine regulator of the rat ovarian theca cell compartment, Biol. Reprod. 64 (2001) 1080–1089, https://doi.org/10.1095/biolreprod64.4.1080.
[77] M.K. O'Bryan, L.M. Foulds, J.F. Cannon, et al., Identification of a novel apolipoprotein, ApoN, in ovarian follicular fluid, Endocrinology 145 (2004) 5231–5242, https://doi.org/10.1210/en.2004-0630.
[78] M. Mann, Can proteomics retire the Western blot? J. Proteome Res. 7 (2008) 3065, https://doi.org/10.1021/pr800463v.
[79] D. Mehta, A.H. Ahkami, J. Walley, S.L. Xu, R.G. Uhrig, The incongruity of validating quantitative proteomics using western blots, Nat. Plants 8 (2022) 1320–1321, https://doi.org/10.1038/s41477-022-01314-8.
[80] S. Wang, A. Collins, A. Prakash, et al., Integrated proteomics analysis of baseline protein expression in pig tissues, J. Proteome Res. 23 (2024) 1948–1959, https://doi.org/10.1021/acs.jproteome.3c00741.
[81] R.F. Savaris, J.M. Groll, S.L. Young, et al., Progesterone resistance in PCOS endometrium: a microarray analysis in clomiphene citrate-treated and artificial menstrual cycles, J. Clin. Endocrinol. Metab. 96 (2011) 1737–1746, https://doi.org/10.1210/jc.2010-2600.
[82] O. Muneyyirci-Delale, A. Babinska, V.L. Nacharaju, M. Dalloul, E. Kornecki, Enhanced levels of F11R receptor (F11R/JAM-1/JAM-A) in PCOS patients, Fertil. Steril. 88 (2007) 186, https://doi.org/10.1016/j.fertnstert.2007.07.641.
[83] Y. Perez-Riverol, J. Bai, C. Bandla, et al., The PRIDE database resources in 2022: A hub for mass spectrometry-based proteomics evidences, Nucleic Acids Res. 50 (2022) D543–D552, https://doi.org/10.1093/nar/gkab1038.